NASA/CR–2014-218249

Calibration of International Space Station (ISS) Node 1 Vibro-Acoustic Model—Report 2

Weiguo Zhang and Ravi Raveendra
Comet Technology Corporation, Ann Arbor, Michigan

April 2014

NASA STI Program . . . in Profile

Since its founding, NASA has been dedicated to the advancement of aeronautics and space science. The NASA scientific and technical information (STI) program plays a key part in helping NASA maintain this important role.

The NASA STI program operates under the auspices of the Agency Chief Information Officer. It collects, organizes, provides for archiving, and disseminates NASA's STI. The NASA STI program provides access to the NASA Aeronautics and Space Database and its public interface, the NASA Technical Report Server, thus providing one of the largest collections of aeronautical and space science STI in the world. Results are published in both non-NASA channels and by NASA in the NASA STI Report Series, which includes the following report types:

- TECHNICAL PUBLICATION. Reports of completed research or a major significant phase of research that present the results of NASA Programs and include extensive data or theoretical analysis. Includes compilations of significant scientific and technical data and information deemed to be of continuing reference value. NASA counterpart of peer-reviewed formal professional papers, but having less stringent limitations on manuscript length and extent of graphic presentations.

- TECHNICAL MEMORANDUM. Scientific and technical findings that are preliminary or of specialized interest, e.g., quick release reports, working papers, and bibliographies that contain minimal annotation. Does not contain extensive analysis.

- CONTRACTOR REPORT. Scientific and technical findings by NASA-sponsored contractors and grantees.

- CONFERENCE PUBLICATION. Collected papers from scientific and technical conferences, symposia, seminars, or other meetings sponsored or co-sponsored by NASA.

- SPECIAL PUBLICATION. Scientific, technical, or historical information from NASA programs, projects, and missions, often concerned with subjects having substantial public interest.

- TECHNICAL TRANSLATION. English-language translations of foreign scientific and technical material pertinent to NASA's mission.

Specialized services also include organizing and publishing research results, distributing specialized research announcements and feeds, providing information desk and personal search support, and enabling data exchange services.

For more information about the NASA STI program, see the following:

- Access the NASA STI program home page at *http://www.sti.nasa.gov*

- E-mail your question to help@sti.nasa.gov

- Fax your question to the NASA STI Information Desk at 443-757-5803

- Phone the NASA STI Information Desk at 443-757-5802

- Write to:
  STI Information Desk
  NASA Center for AeroSpace Information
  7115 Standard Drive
  Hanover, MD 21076-1320

NASA/CR–2014-218249

Calibration of International Space Station (ISS) Node 1 Vibro-Acoustic Model—Report 2

Weiguo Zhang and Ravi Raveendra
Comet Technology Corporation, Ann Arbor, Michigan

National Aeronautics and
Space Administration

Langley Research Center
Hampton, Virginia 23681-2199

Prepared for Langley Research Center
under Contract NNL07AA00C

April 2014

Available from:

NASA Center for AeroSpace Information
7115 Standard Drive
Hanover, MD 21076-1320
443-757-5802

1. Introduction

The objective of the present investigation is to correlate the vibration data measured by NASA using acoustic emission, at specific sensor locations on Node 1 of the International Space Station (ISS), to corresponding values predicted by Comet EnFlow, an analysis software for high frequency vibro-acoustic analysis based on Energy Finite Element Method (EFEM) that was developed previously as a result of an SBIR funding from NASA LaRC. Previously, analysis performed based on a source located at sensor location 13 was reported. In this report, responses due to sources located at additional locations are evaluated and compared to measurements. The source and sensor locations used in the present study are shown in Figure 1. The measured data sets due to sources at locations 10, 2, 11, 8 and 5 are provided by NASA. Sources 10 and 2 are located at the barrel section of the model. Source 11 is located at port hatch. Sources 8 and 5 are located at forward cone and aft cone, respectively.

Sensors that were used in the previously reported study are also used presently and the measured data are processed similarly. However, unlike source 13 which was generated by an actual leak, the sources investigated in this study were driven by a piezoelectric sensor to simulate the leak. Further, the sensors were not placed very close to the source location and as a result it is not feasibly to obtain input power accurately as before. The approximate total input power generated through the excitation at the source locations are computed based on the response of the closet sensor. Additionally, the sources are decomposed into direct and reverberant fields with associated regions (areas) as was done in the second part of the previously reported analysis. Also, the damping coefficients identified in previous work are utilized in the present study.

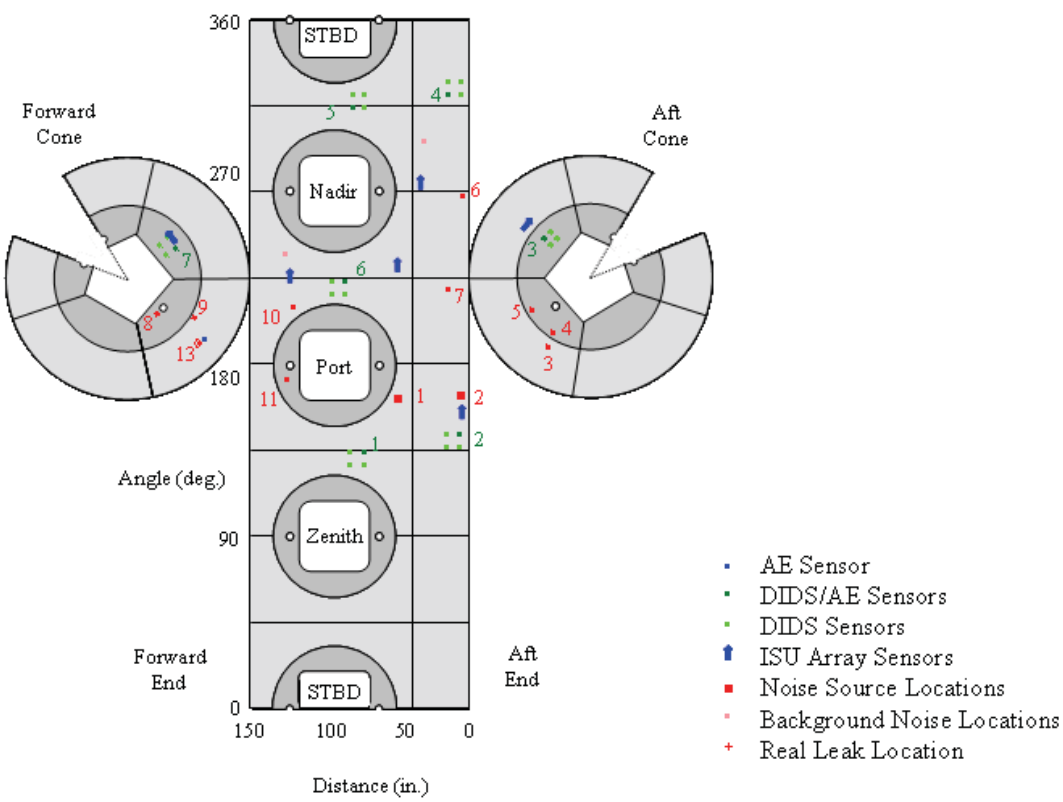

Figure 1.1 Source and Sensor Locations on Node 1 Wall

2. Results

The calibration results corresponding to sources 10, 2, 11, 8 and 5 are sequentially presented.

2.1 Source 10

The locations of source 10 and sensor 6 are shown in Figure 2.1.1. The direct field region is taken to be the pink area around source 10 (note that the sensor location is outside the direct field region. The reverberant filed generated at the boundary of the pink patch is transmitted to the other parts of the model. The approximate total input power generated through the excitation at source 10 location is computed based on the response of the sensor 6. The flexural velocities computed at all sensor locations using Comet EnFlow are compared to measured velocities in Figures 2.1.2 - 2.1.8. These figures are arranged according to the distance from the sensors to the location of excitation (from near to far).

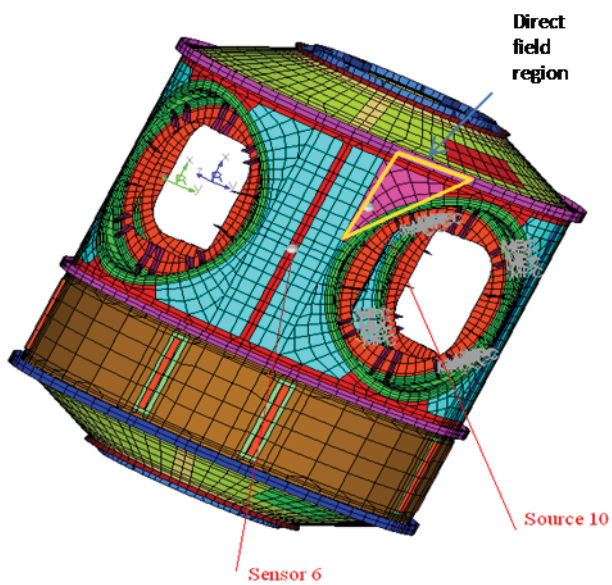

Figure 2.1.1 Source 10 location

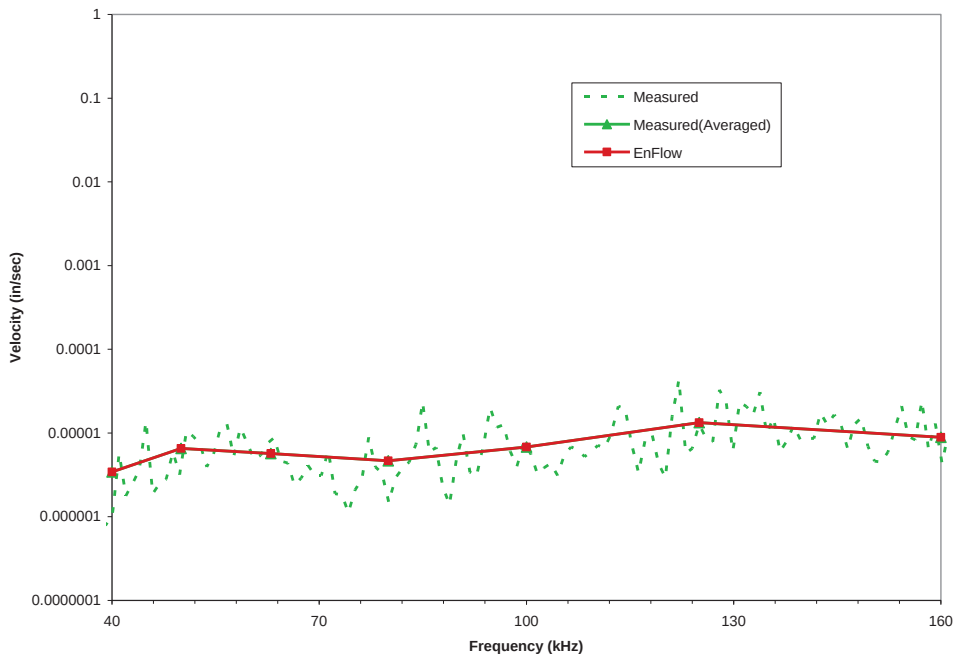

Figure 2.1.2 Flexural Velocity of Sensor 6

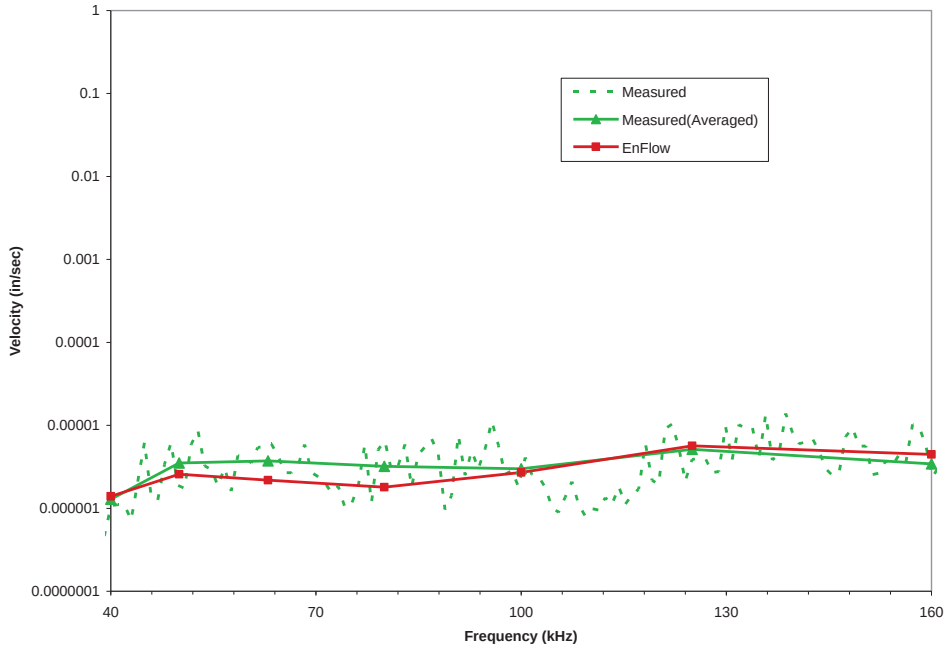

Figure 2.1.3 Flexural Velocity of Sensor 1

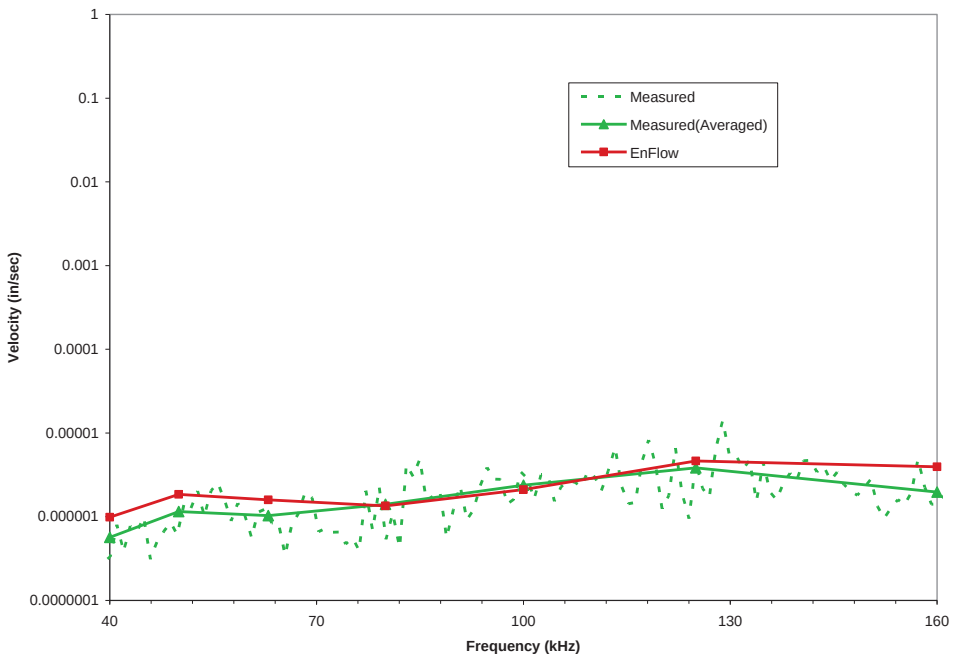

Figure 2.1.4 Flexural Velocity of Sensor 2

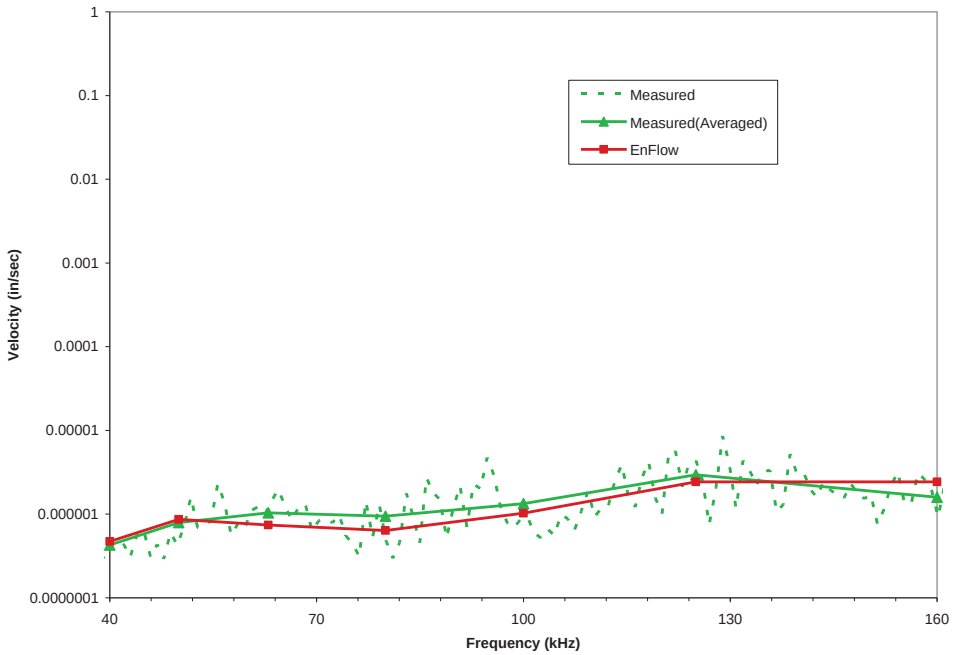

Figure 2.1.5 Flexural Velocity of Sensor 4

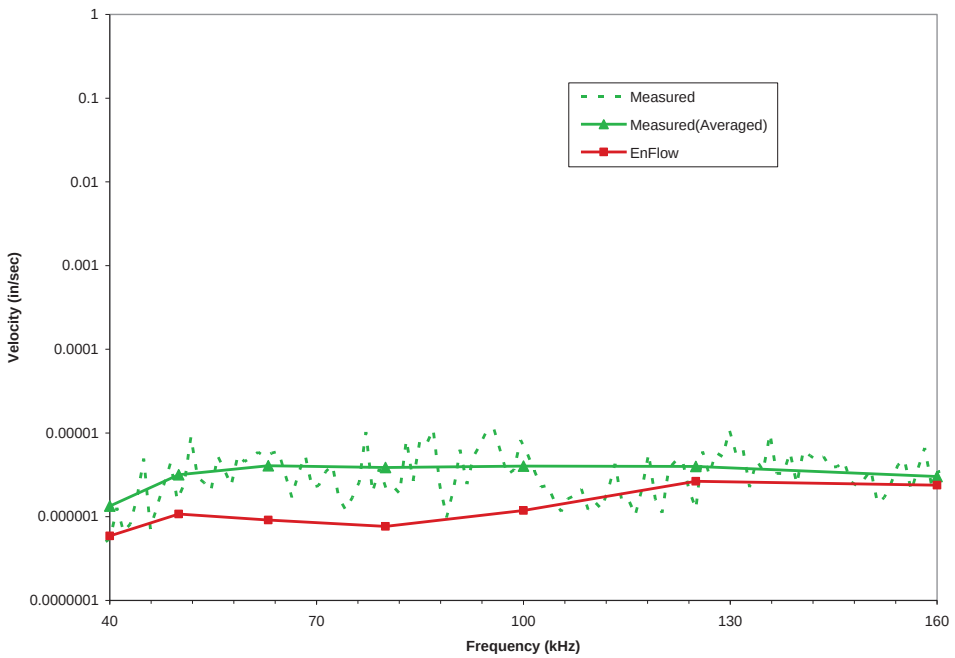

Figure 2.1.6 Flexural Velocity of Sensor 5

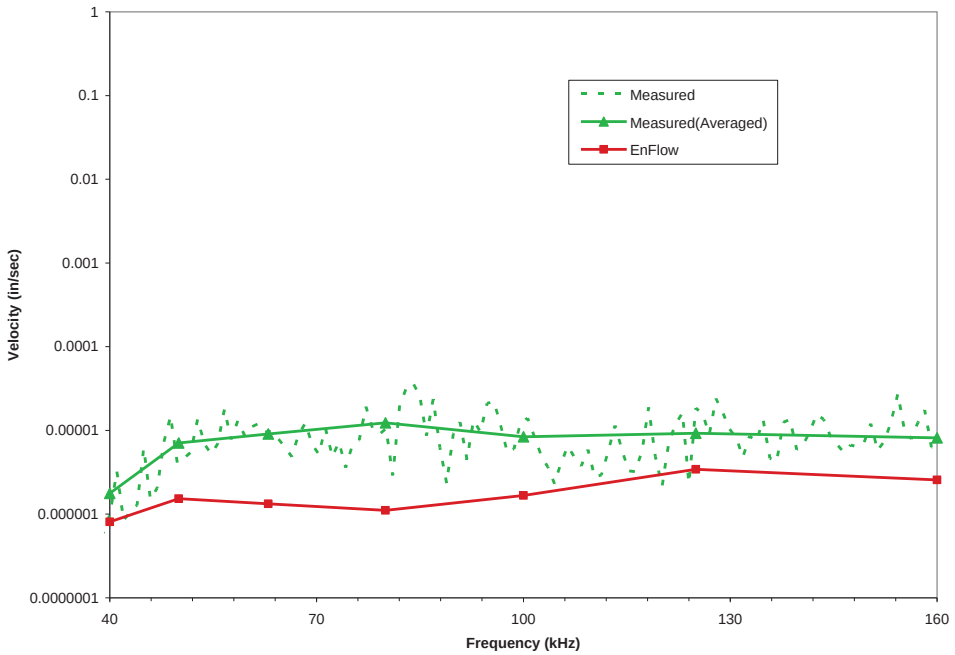

Figure 2.1.7 Flexural Velocity of Sensor 7

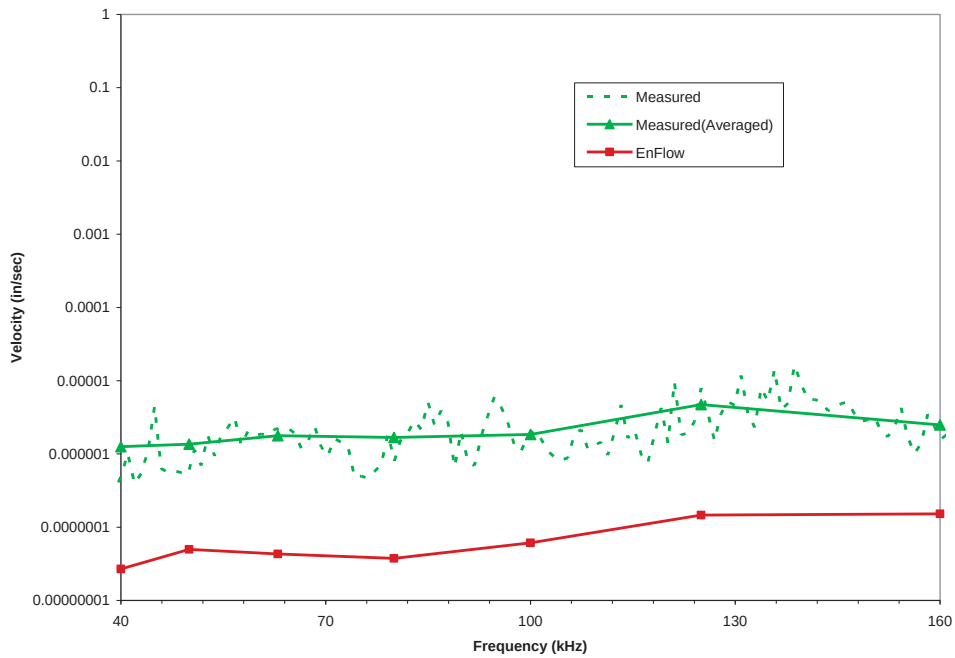

Figure 2.1.8 Flexural Velocity of Sensor 3

2.2 Source 2

The locations of source 2 and sensor 2 are shown in Figure 2.2.1. The approximate total input power generated through the excitation at source 2 location is computed based on the response of the sensor 2. The direct field is included in the pink area surrounding source 2. The reverberant filed is generated at the edge of the pink area. As in the previous case, the sensor is located outside the direct field region. The flexural velocities at all sensor locations are compared as before in Figures 2.2.2 - 2.2.8.

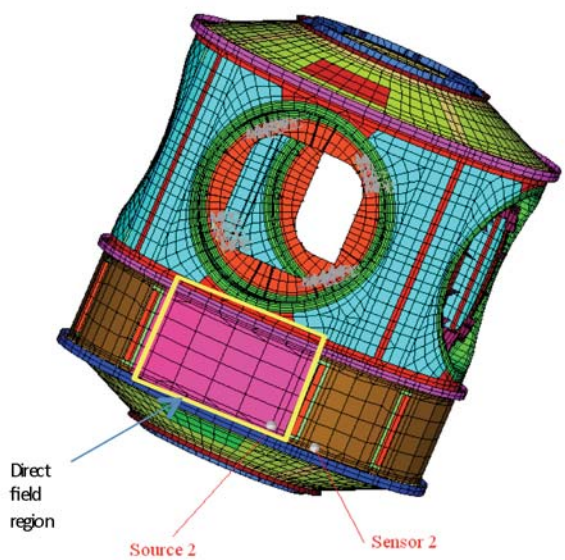

Figure 2.2.1 Source 2 location

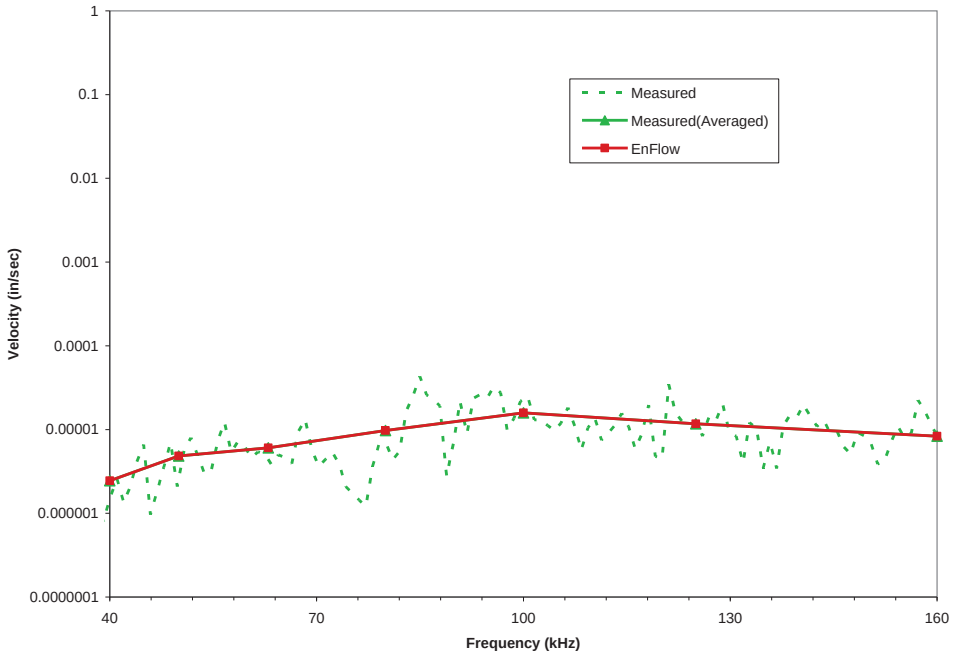

Figure 2.2.2 Flexural Velocity of Sensor 2

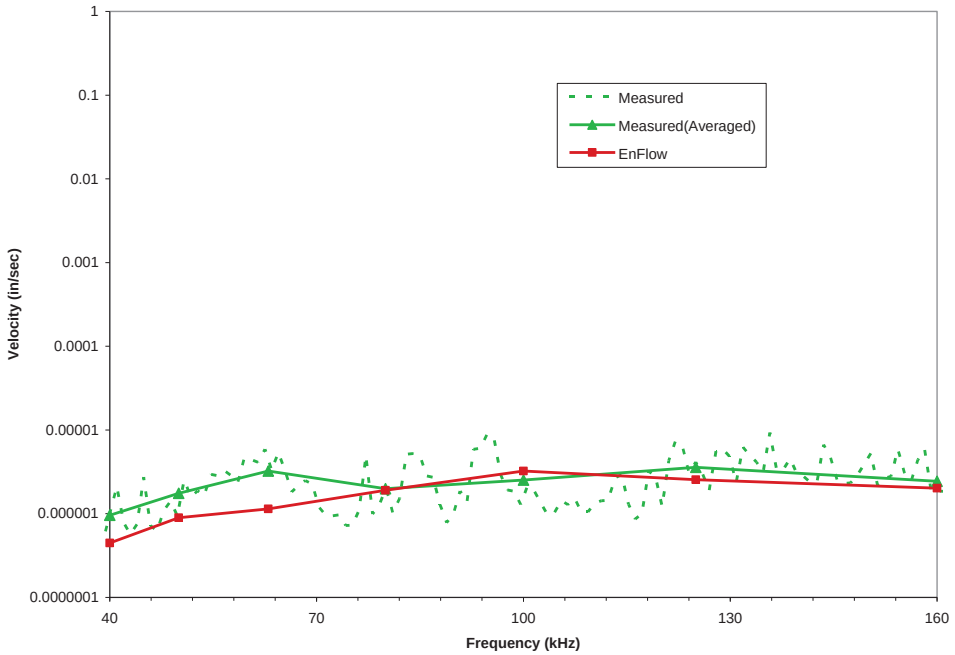

Figure 2.2.3 Flexural Velocity of Sensor 1

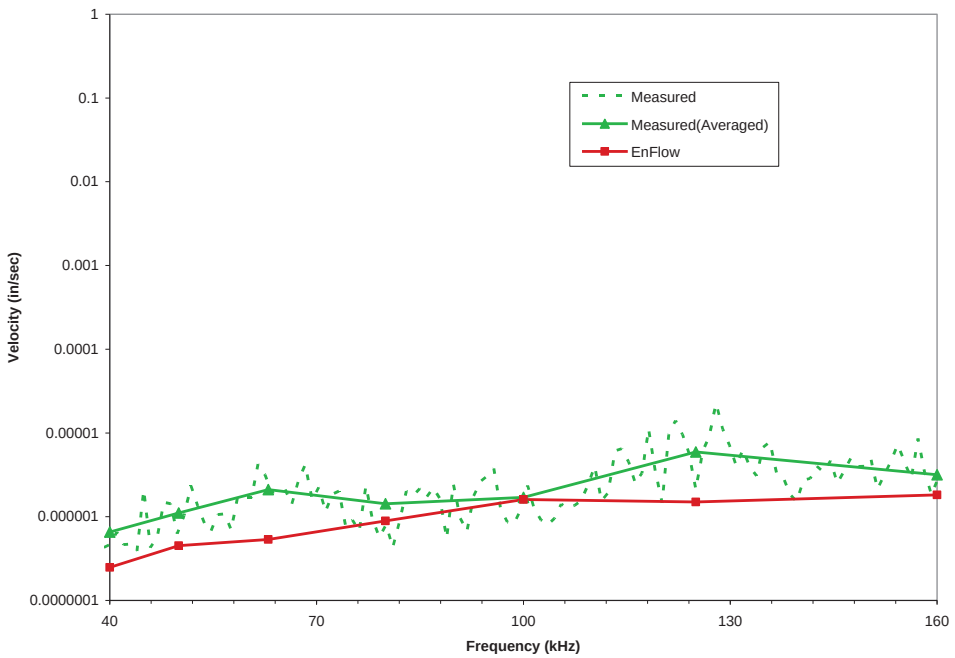

Figure 2.2.4 Flexural Velocity of Sensor 4

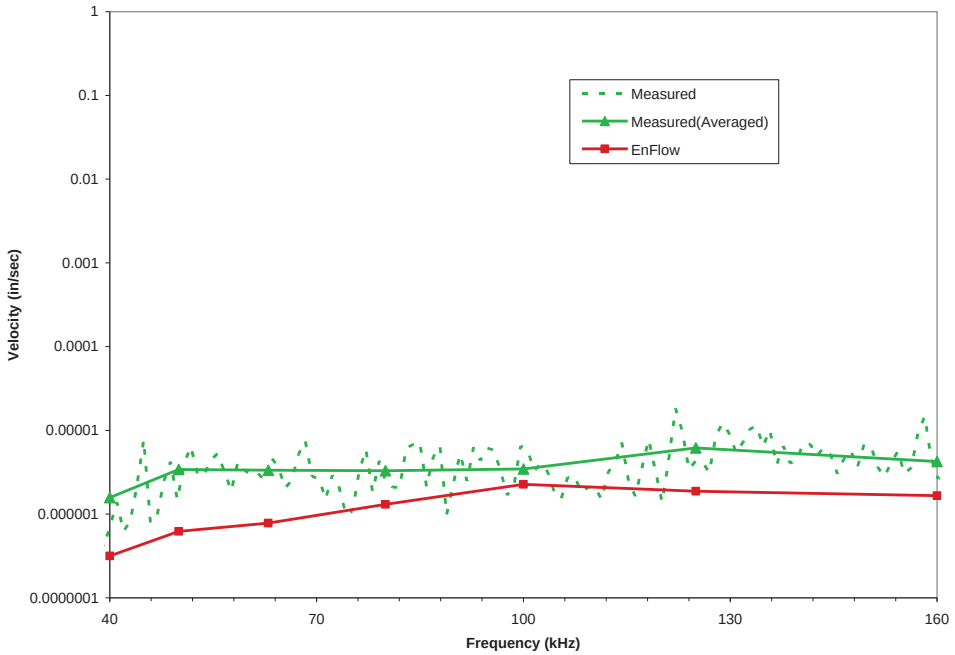

Figure 2.2.5 Flexural Velocity of Sensor 6

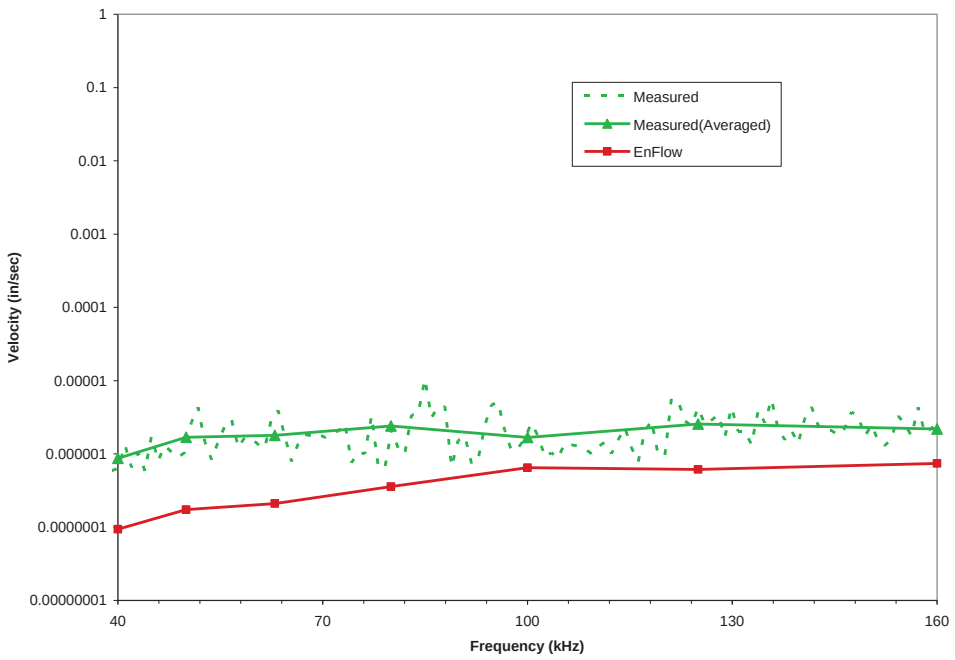

Figure 2.2.6 Flexural Velocity of Sensor 5

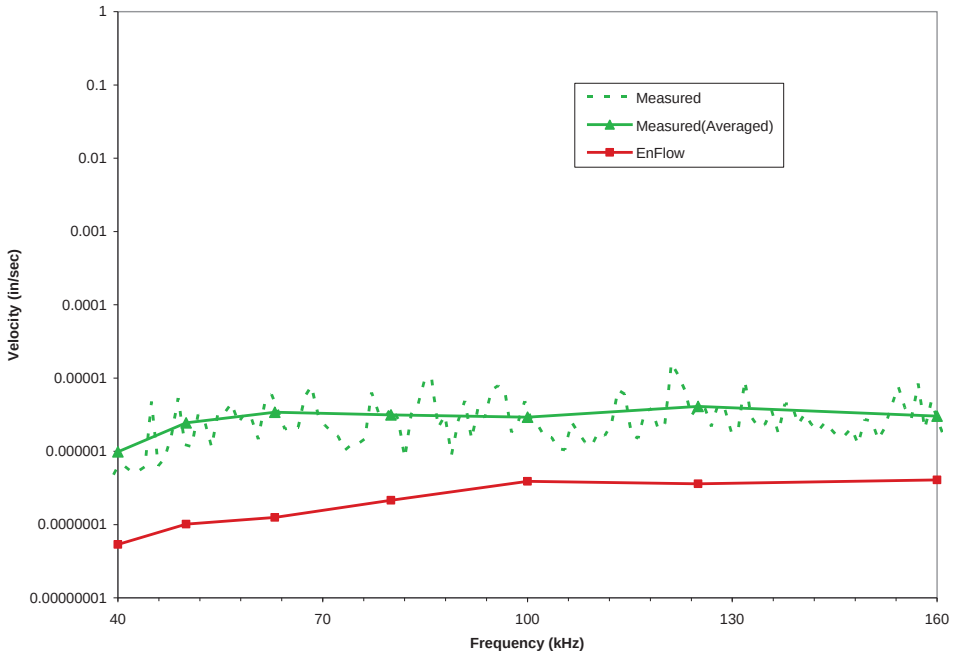

Figure 2.2.7 Flexural Velocity of Sensor 7

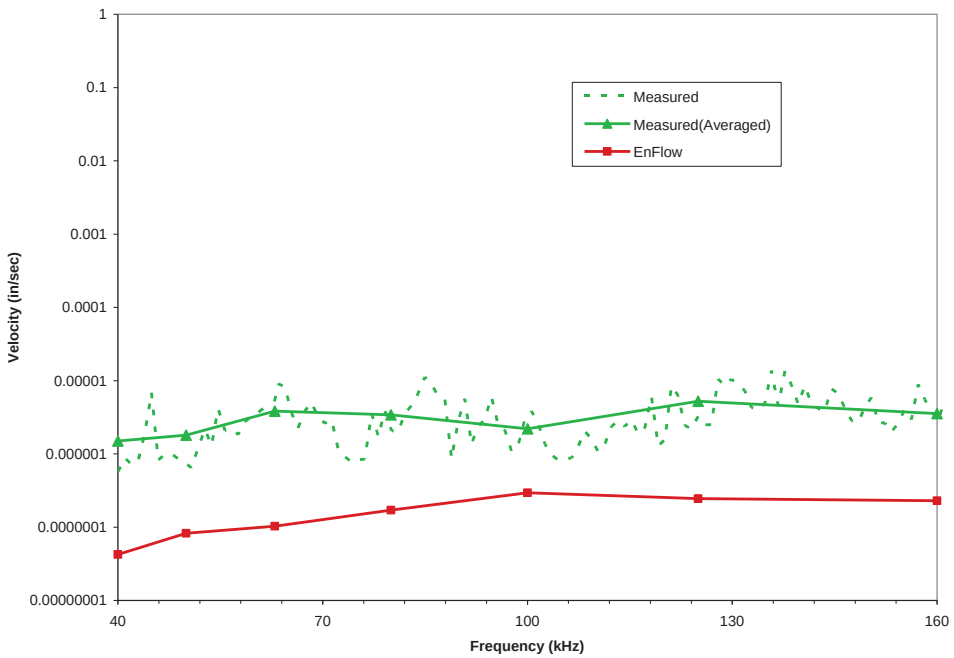

Figure 2.2.8 Flexural Velocity of Sensor 3

2.3 Source 11

As indicated in the previous report, responses (flexural velocities) can be predicted using (a) total field, or (b) decomposed fields (i.e. by separating the total field into direct and reverberant fields). Previous analysis, presented in the first report, has indicated that the decomposition of the total field into direct and reverberant fields improves the accuracy of the predicted responses. When decomposing the total field, typically, the direct field region is assumed to be a small patch of area around the source. In order to estimate the source and subsequently the responses accurately, the sensor location must be within the direct field region (preferably very close to the source location). However, in the present study, the source and sensor locations are not close to each other and as a result the sensors could not be located within the direct field region. In these situations, it is expected that the responses predicted using total and decomposed field will be similar (this is confirmed by the investigation reported in the Appendix of this report). As a consequence, analyses are performed using total fields without decomposition in the current and the ensuing cases.

The locations of source 11 and sensor 1 are shown in Figure 2.3.1. The approximate total input power generated through the excitation at source 11 location is computed based on the response of the sensor 1. As shown in Appendix A, the velocities predicted using total field without decomposition and decomposition of the total field into direct and reverberant fields does not make noticeable difference. Thus, the flexural velocities at all sensor locations are computed using total field and these are compared to measurements in Figures 2.3.2 - 2.3.8.

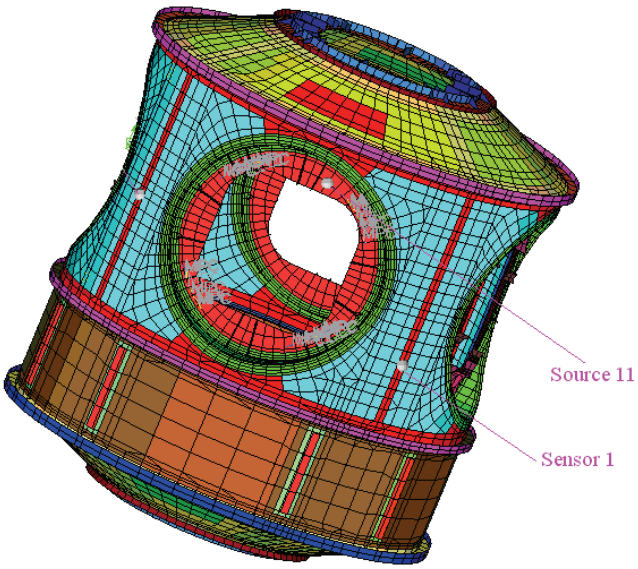

Figure 2.3.1 Source 11 location

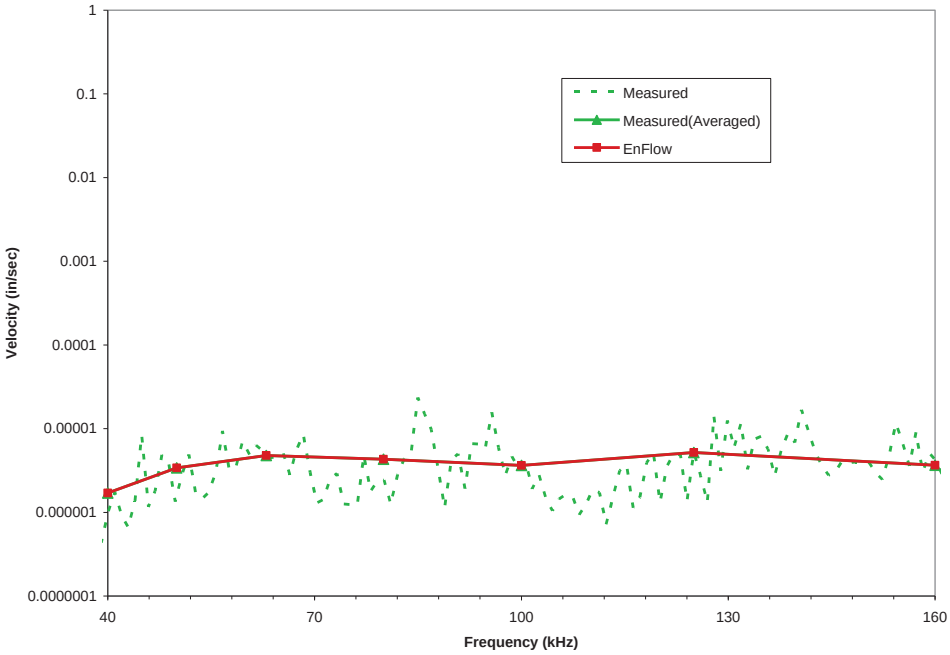

Figure 2.3.2 Flexural Velocity of Sensor 1

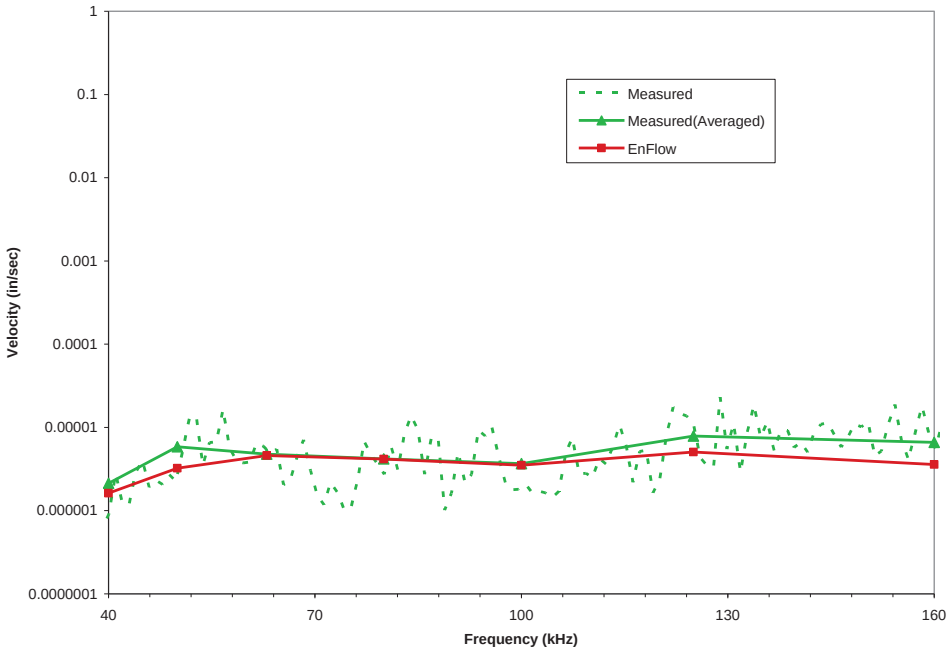

Figure 2.3.3 Flexural Velocity of Sensor 6

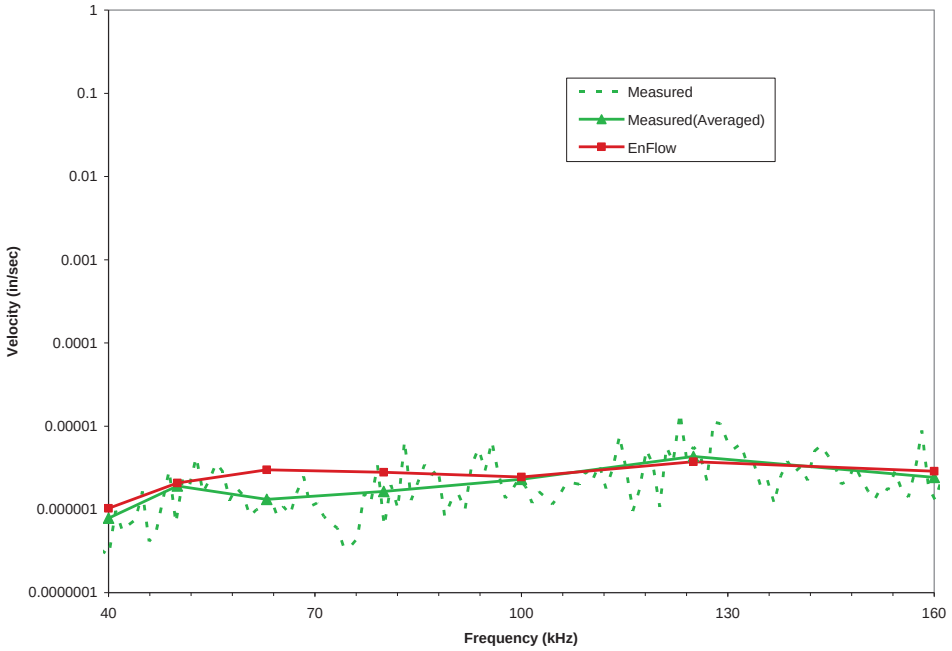

Figure 2.3.4 Flexural Velocity of Sensor 2

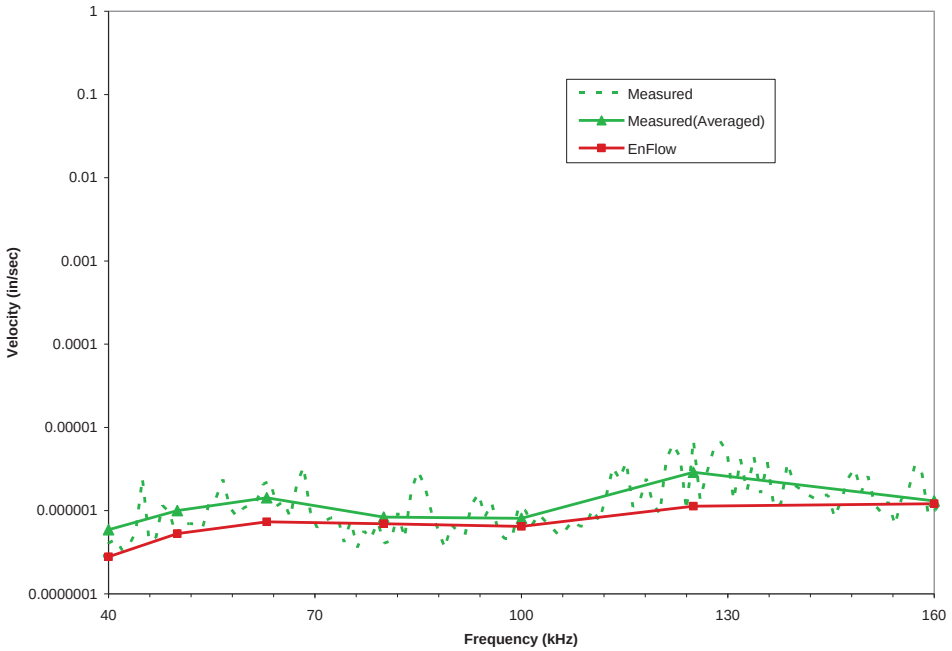

Figure 2.3.5 Flexural Velocity of Sensor 4

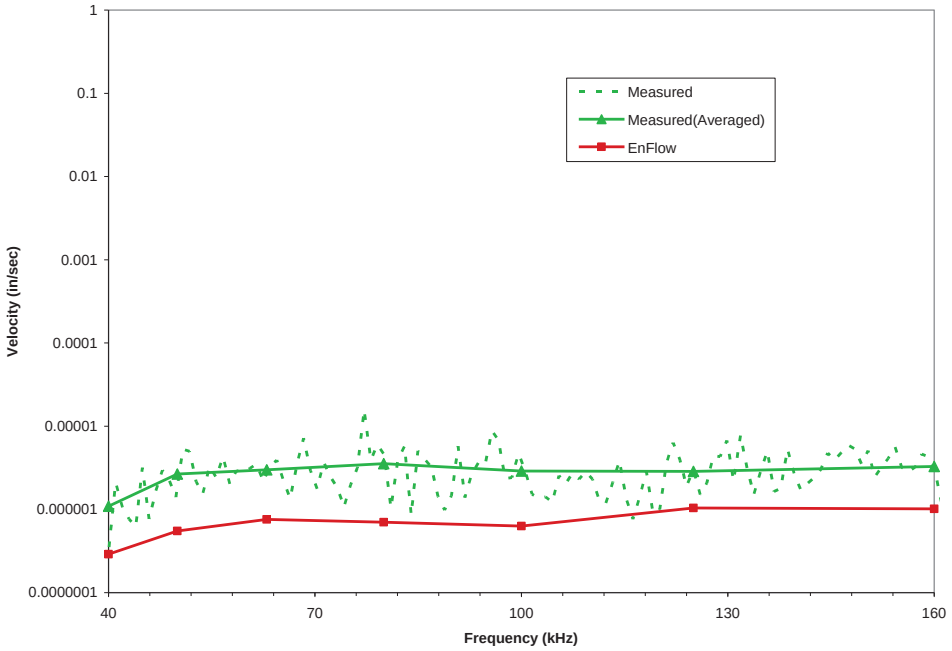

Figure 2.3.6 Flexural Velocity of Sensor 5

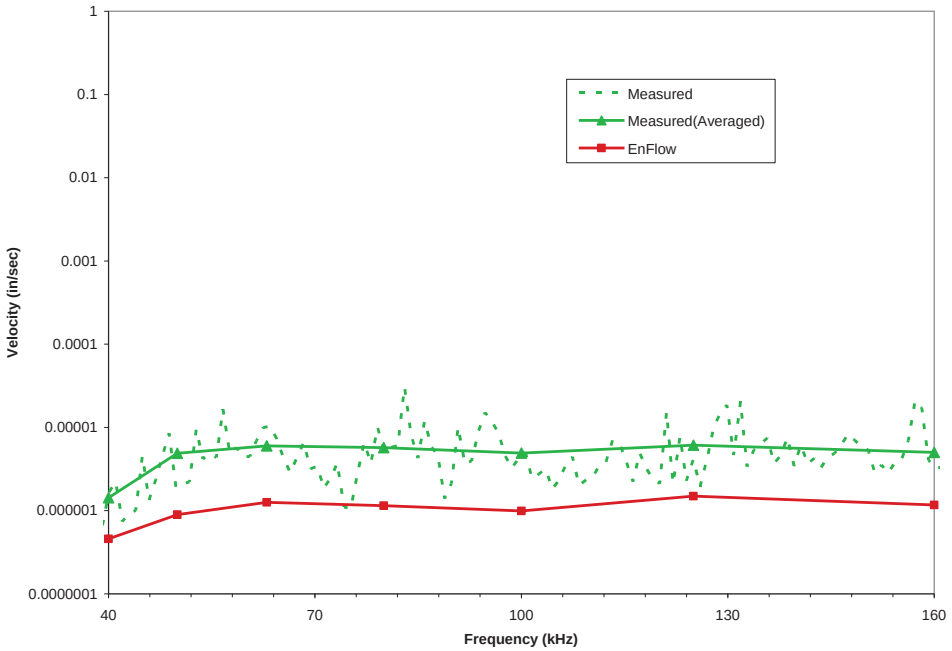

Figure 2.3.7 Flexural Velocity of Sensor 7

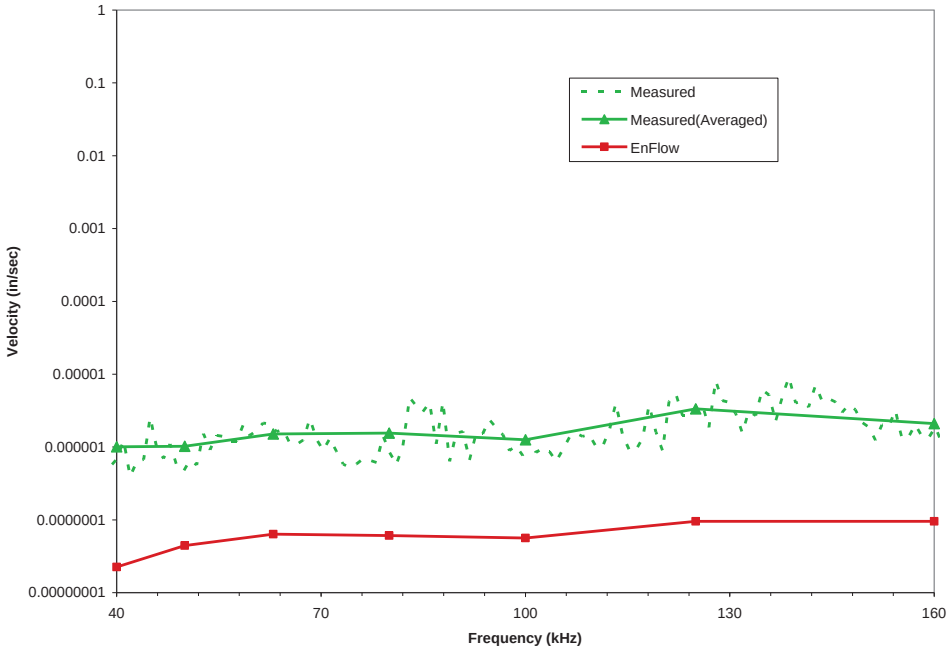

Figure 2.3.8 Flexural Velocity of Sensor 3

2.4 Source 8

The locations of source 8 and sensor 7 are shown in Figure 2.4.1. The approximate total input power generated through the excitation at source 8 location is computed based on the response of the sensor 7. The flexural velocities at all sensor locations are compared in Figures 2.4.2 - 2.4.8.

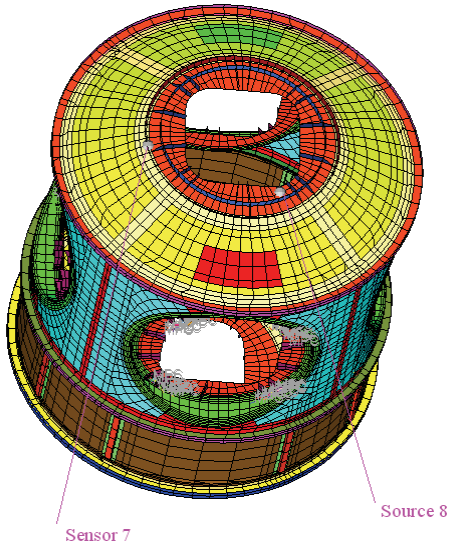

Figure 2.4.1 Source 8 location

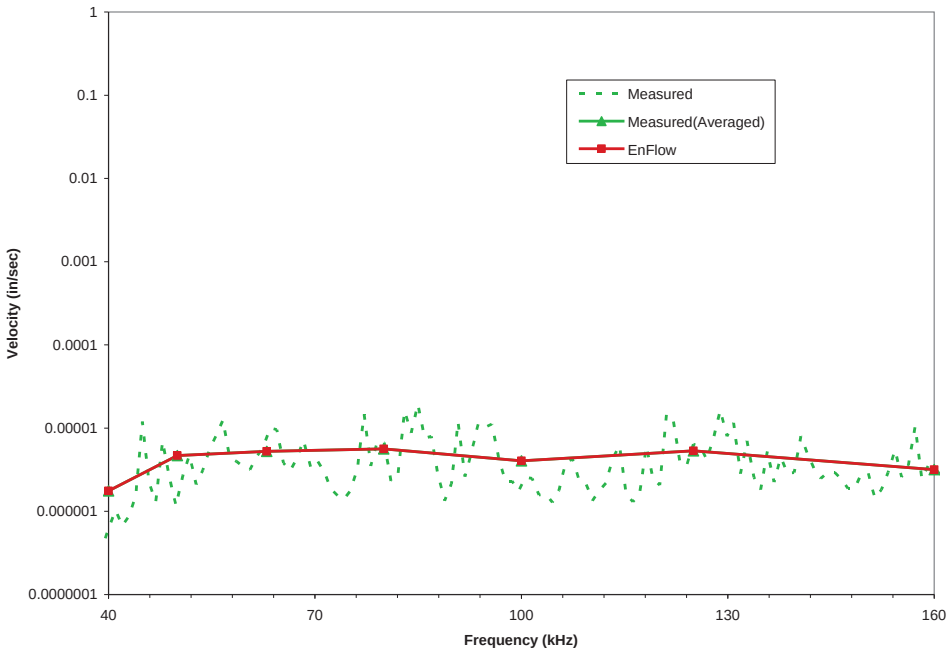

Figure 2.4.2 Flexural Velocity of Sensor 7

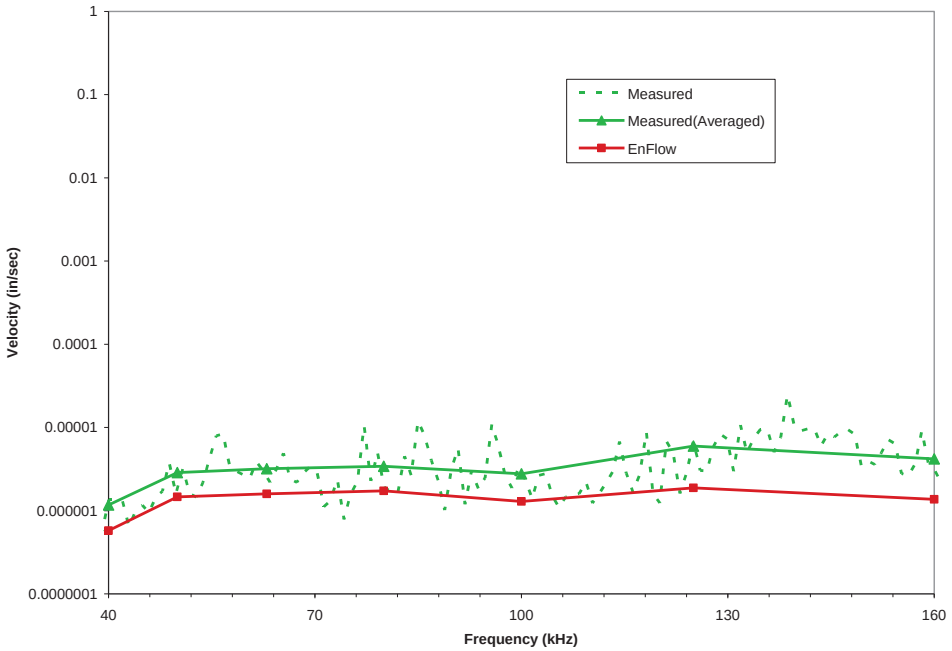

Figure 2.4.3 Flexural Velocity of Sensor 1

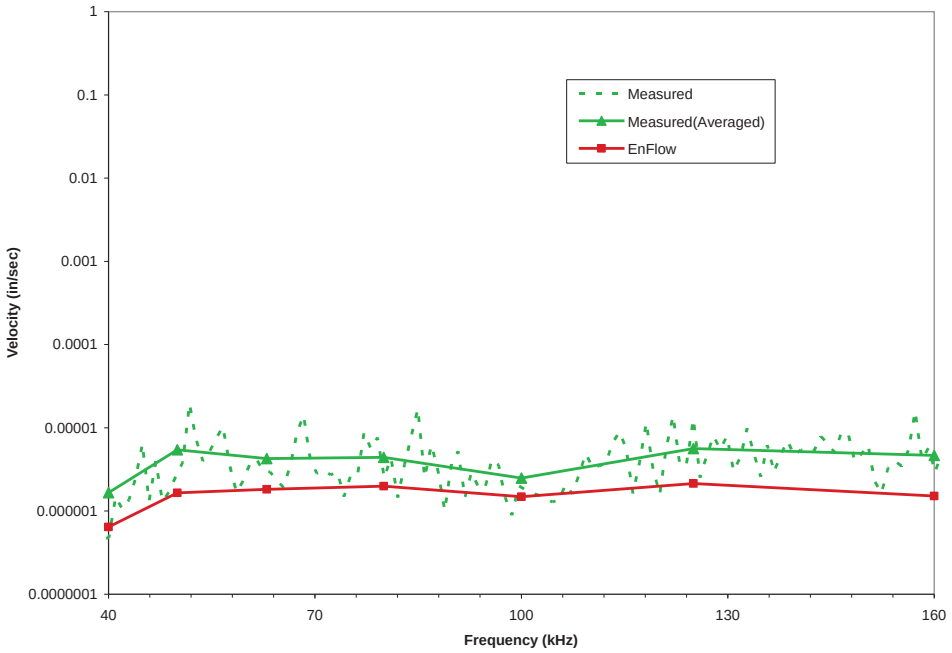

Figure 2.4.4 Flexural Velocity of Sensor 6

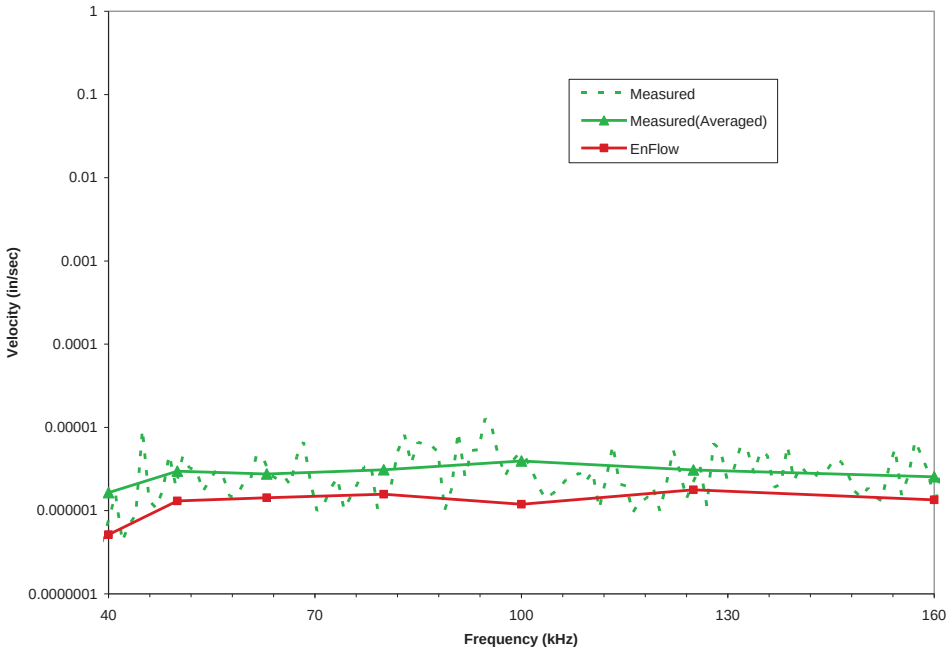

Figure 2.4.5 Flexural Velocity of Sensor 5

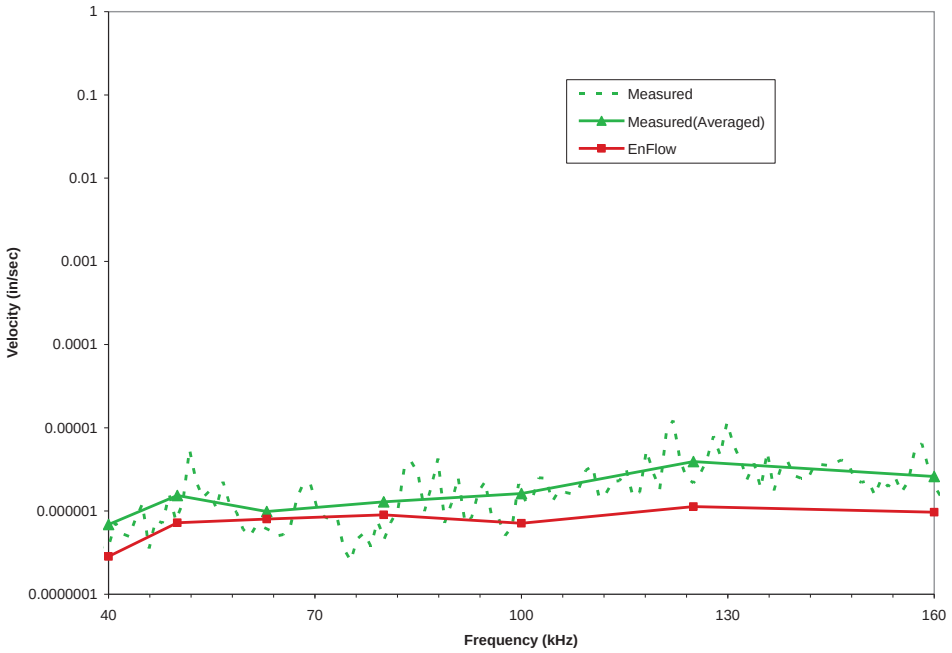

Figure 2.4.6 Flexural Velocity of Sensor 2

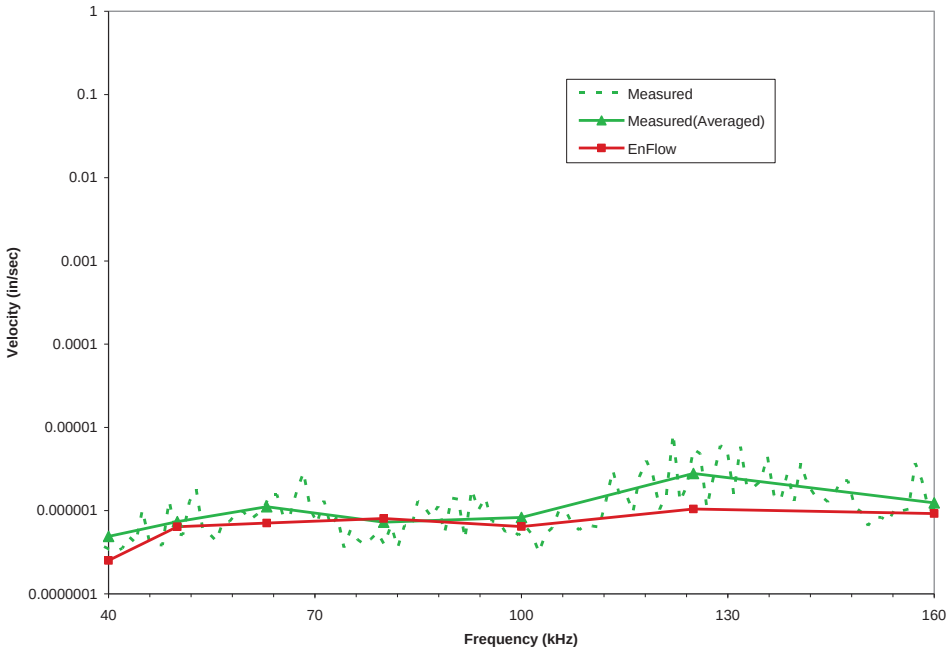

Figure 2.4.7 Flexural Velocity of Sensor 4

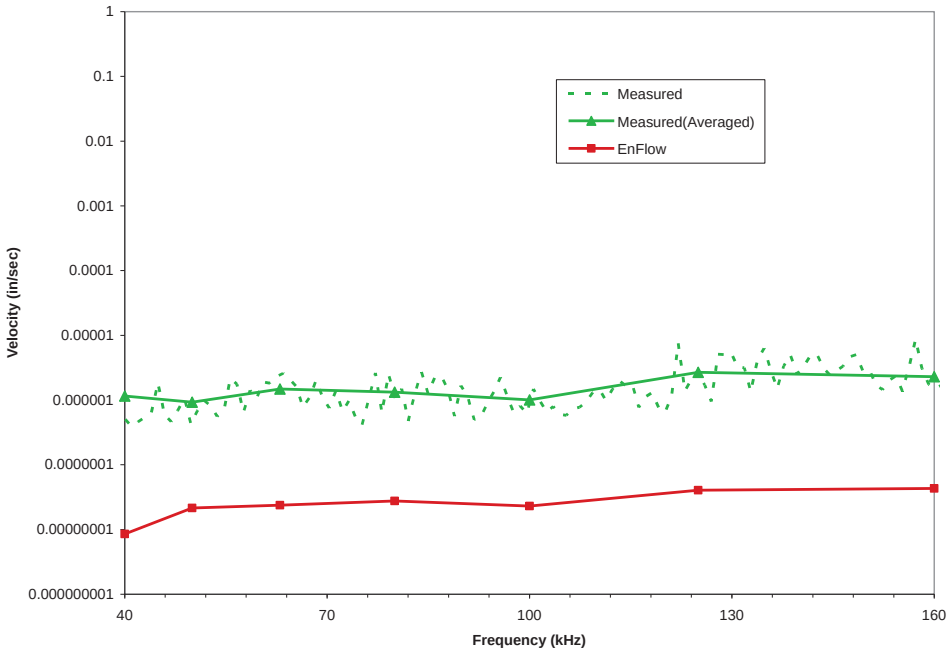

Figure 2.4.8 Flexural Velocity of Sensor 3

2.5 Source 5

The locations of source 5 and sensor 3 are shown in Figure 2.5.1. The approximate total input power generated through the excitation at source 5 location is computed based on the response of the sensor 3. The flexural velocities at all sensor locations are compared in Figures 2.5.2 - 2.5.8.

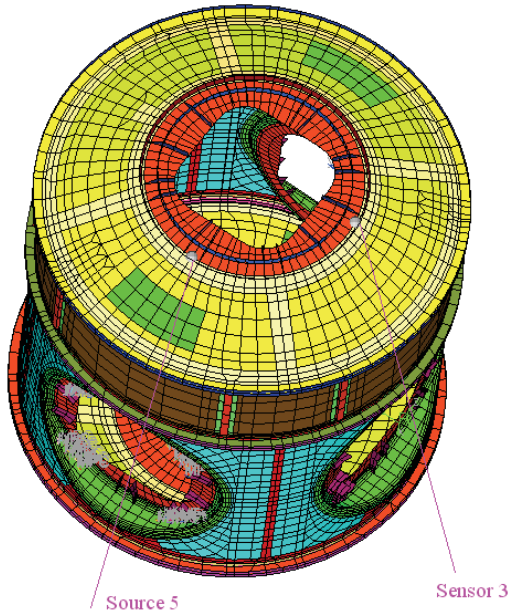

Figure 2.5.1 Source 5 location

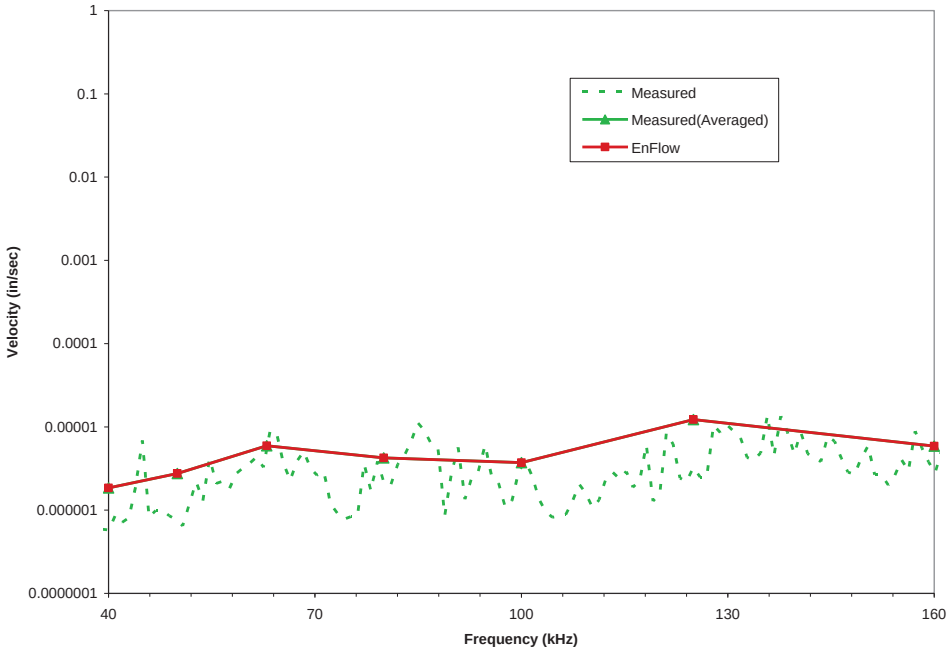

Figure 2.5.2 Flexural Velocity of Sensor 3

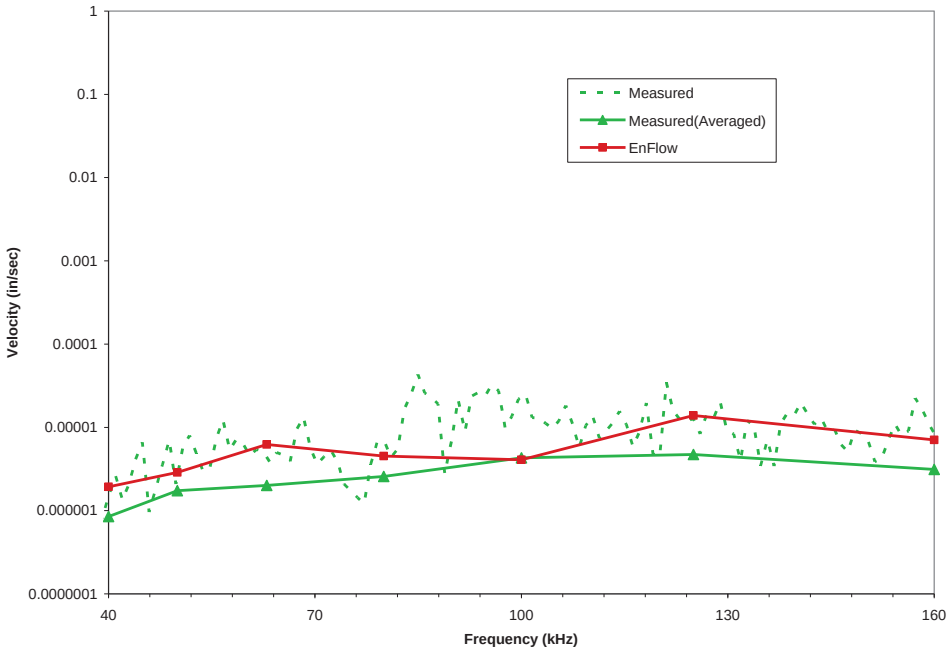

Figure 2.5.3 Flexural Velocity of Sensor 2

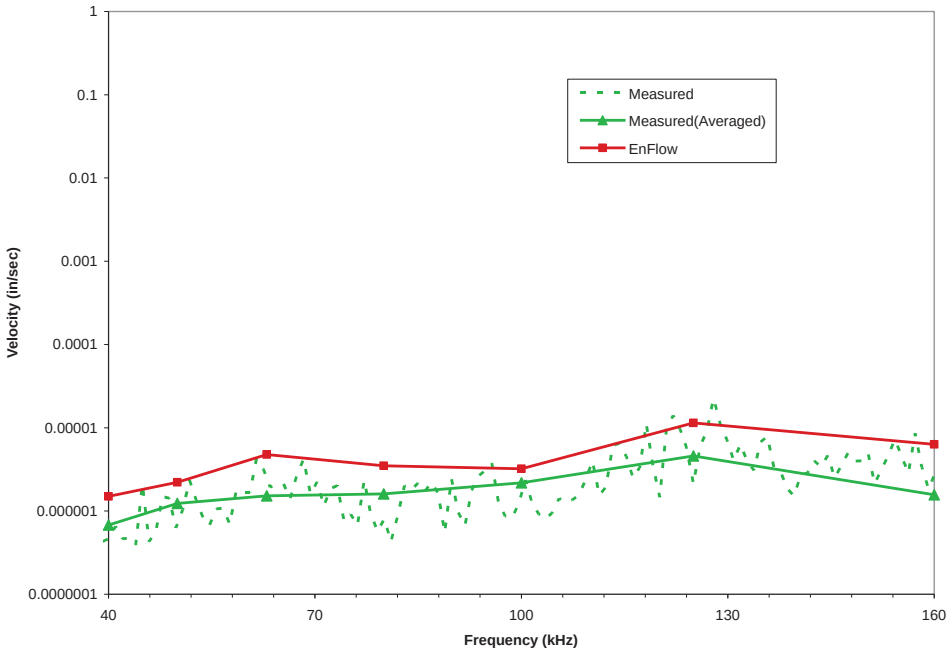

Figure 2.5.4 Flexural Velocity of Sensor 4

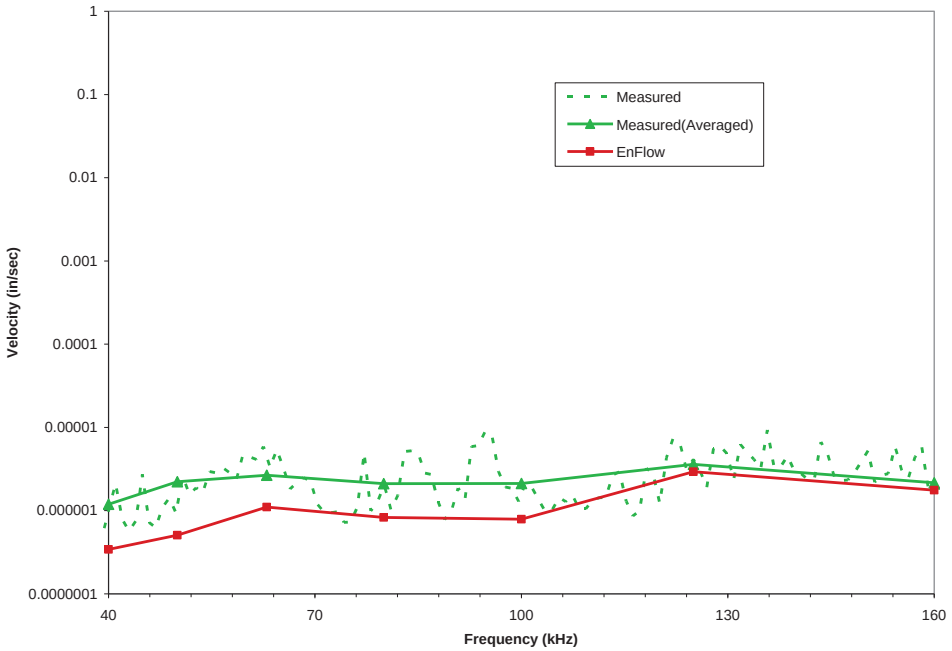

Figure 2.5.5 Flexural Velocity of Sensor 1

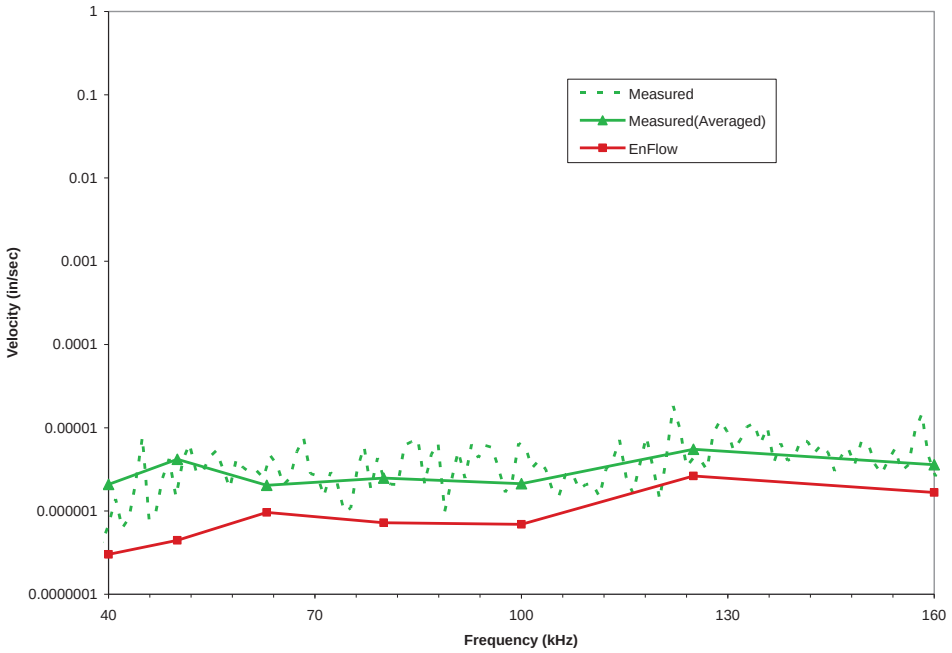

Figure 2.5.6Flexural Velocity of Sensor 6

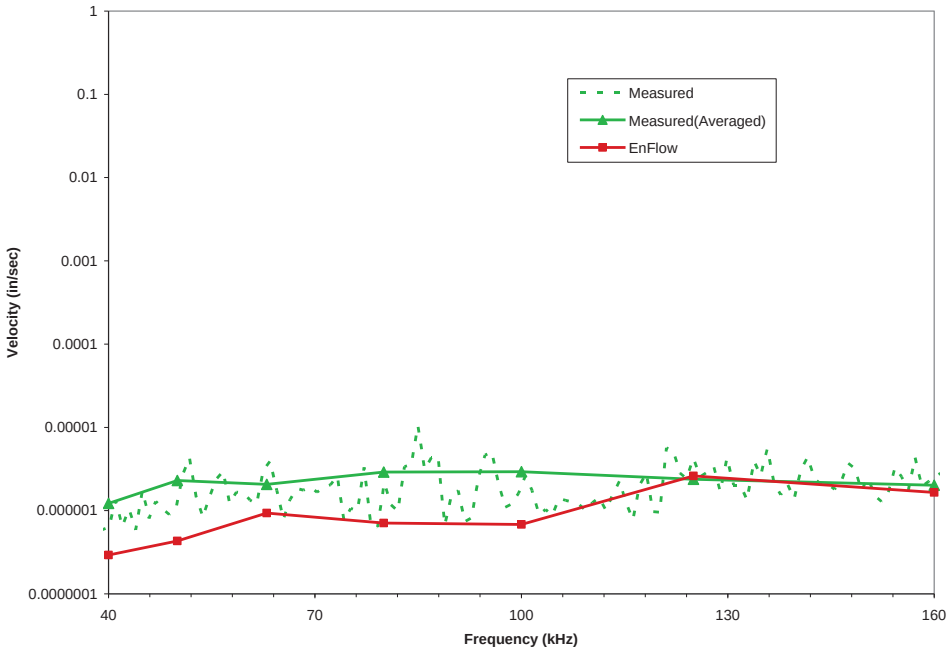

Figure 2.5.7 Flexural Velocity of Sensor 5

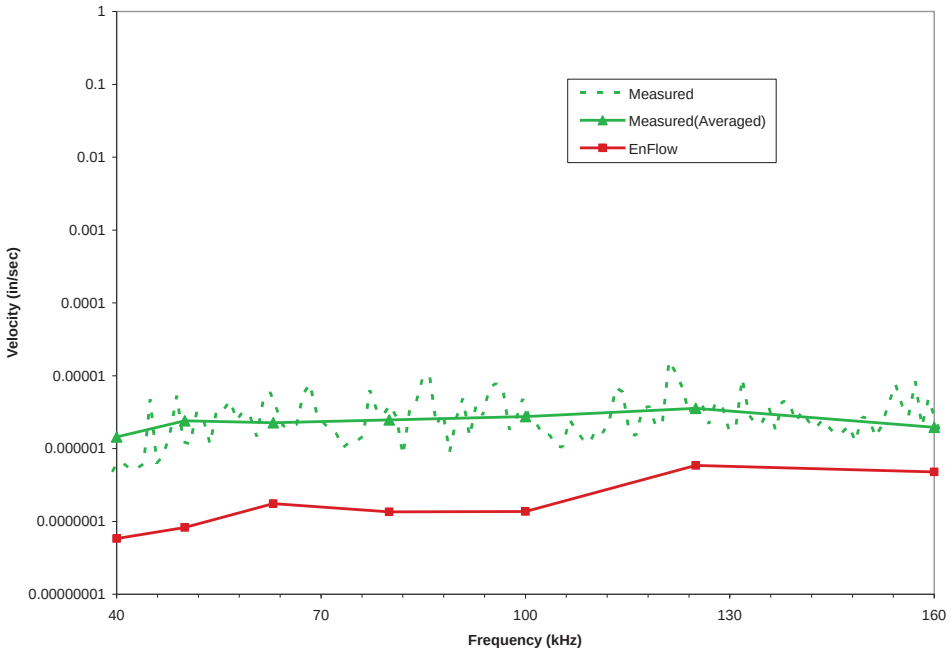

Figure 2.5.8 Flexural Velocity of Sensor 7

3. Discussion

Overall, good correlations are observed at sensors on the barrel section for all sources. The correlations are better when location of sensor is close to the source location. In the present study, the source locations are not in the neighborhood of the sensor location. Additionally, in some case, junctions also exist between the sources and the sensor and therefore input power is further approximated due to the incorporation of the effect of energy transfer at the junction. Nevertheless, good correlations in most cases indicate that the input power is estimated properly. However, the correlations between measured and predicted results at sensors 7 and 3 are not as good. These two sensors are located at the two end cones, which have relatively complex configurations. In some cases, it is observed that the measured responses at these two sensors are higher than the responses at locations, which are closer to the source. The higher response indicates the injection of additional power at the termination of the end cone. The modeling of this effect may require the modification of the (end) boundary conditions in the EnFlow model to include the additional power. Furthermore, the support frame is connected with the Node 1 model through four pins at two end cones (see Figure 3.1). Although the frame is very stiff, it is possible some energy is transferred between the end cones through the frame. Some additional feature development in EnFlow is necessary to incorporate this energy transfer mechanism by special joints without modeling the frame explicitly.

Figure 3.1 Support structure of Node 1

Appendix

A.1 The direct field effect

When the sensors used to estimate the input power are outside the direct field regions as in the present investigation, the decomposition of the total field into direct and reverberant fields does not have much effect on the responses. This is illustrated by studying the responses due to source 10 studied in Section 2.1. The approximate input power at the location of excitation with and without direct field is compared in Figure A.1. Both computations are based on the measured response at sensor 6, which is outside the direct field region.

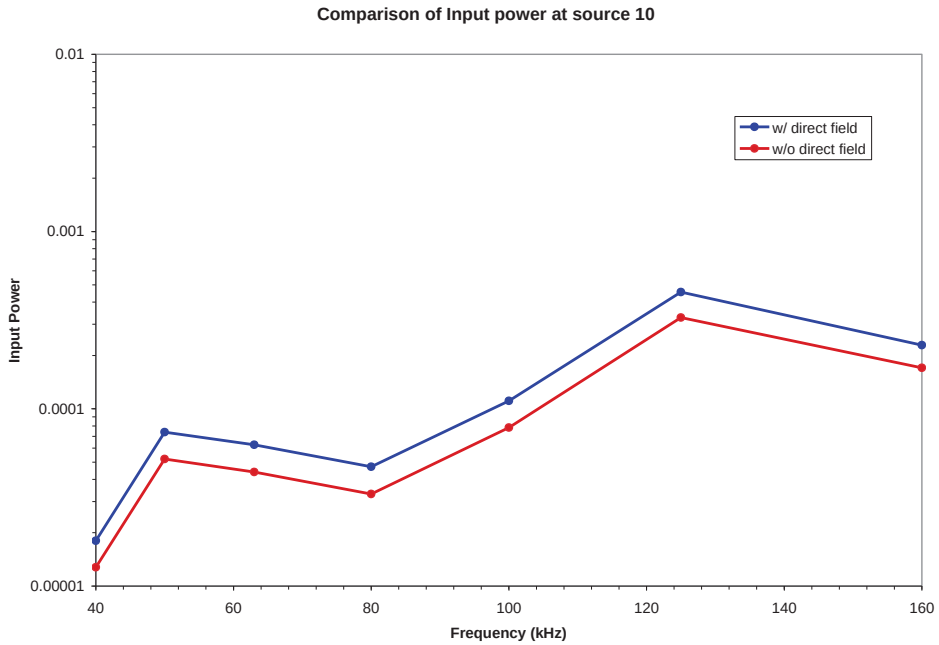

Figure A.1 Input power comparison at source 10

It can be seen that the input power from incorporating direct field is higher than the power neglecting the direct field. This is expected since some portion of total input power is dissipated as direct waves within the direct field region. The response at sensor 6 is generated only by the reverberant portion of the total input power. When the direct field is neglected, the total input power contributes to the response of sensor 6. The responses, computed at all sensors using input powers with and without direct field, are compared in Figures A.2 - A.8. As expected, these responses are almost identical (note that similar results are obtained for all other cases). Thus, it can be concluded that when a sensor, located outside the direct field region, is used to derive the approximate input power, the effect of direct field is not important. In order to evaluate accurate input power more accurately by incorporating the direct field, the sensor should be placed close to the source location (i.e. the source and sensor should be located within the direct field region) as demonstrated in the next section.

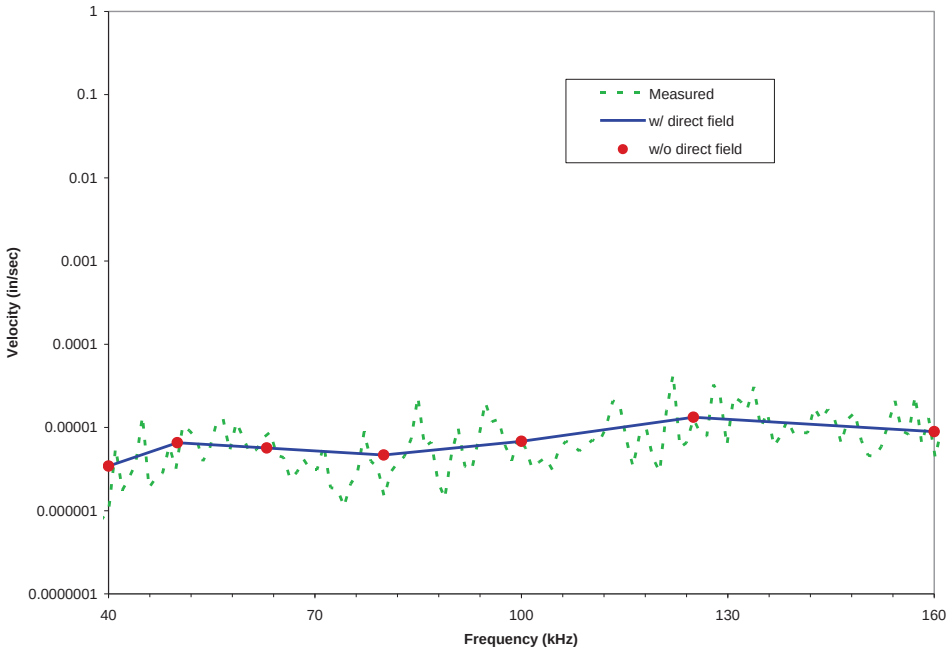

Figure A.2 Comparison at sensor 6

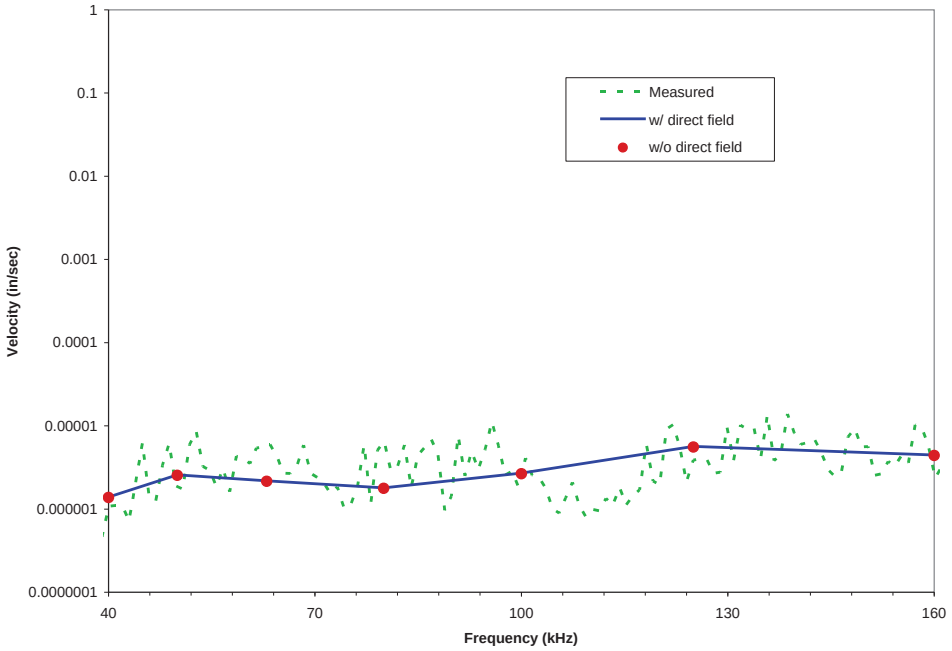

Figure A.3 Comparison at sensor 1

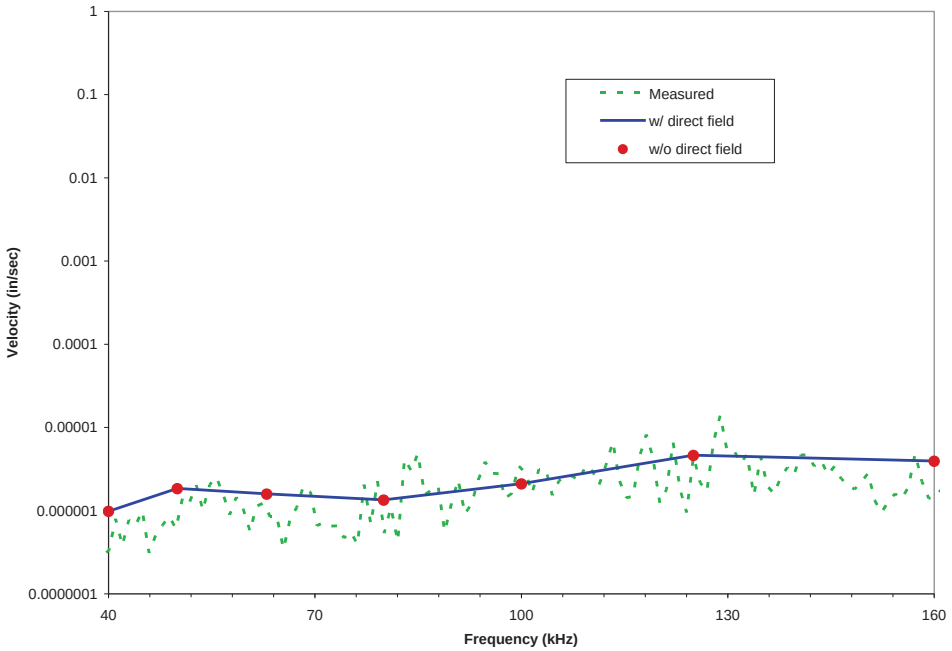

Figure A.4 Comparison at sensor 2

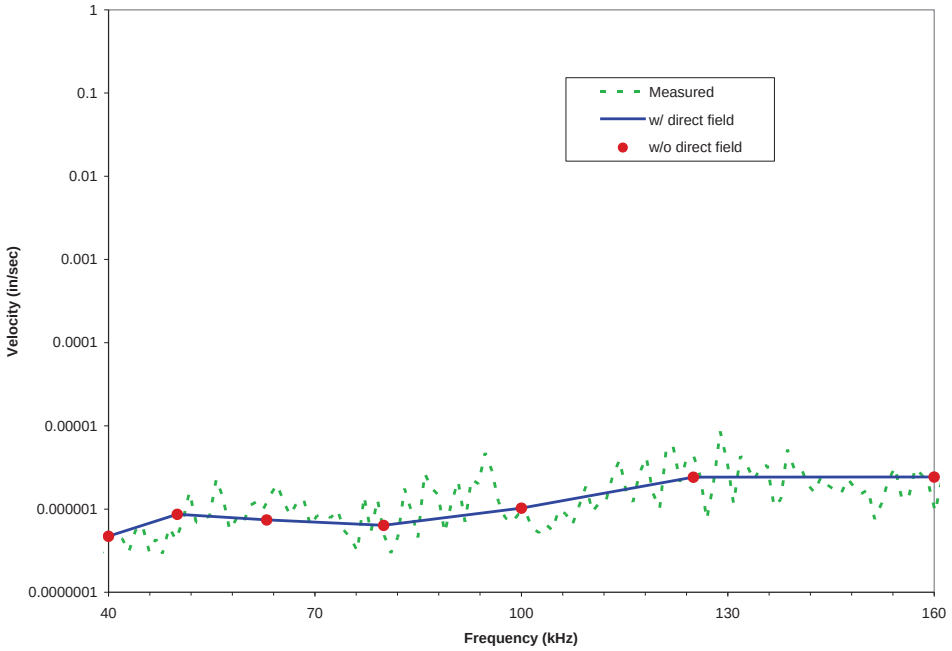

Figure A.5 Comparison at sensor 4

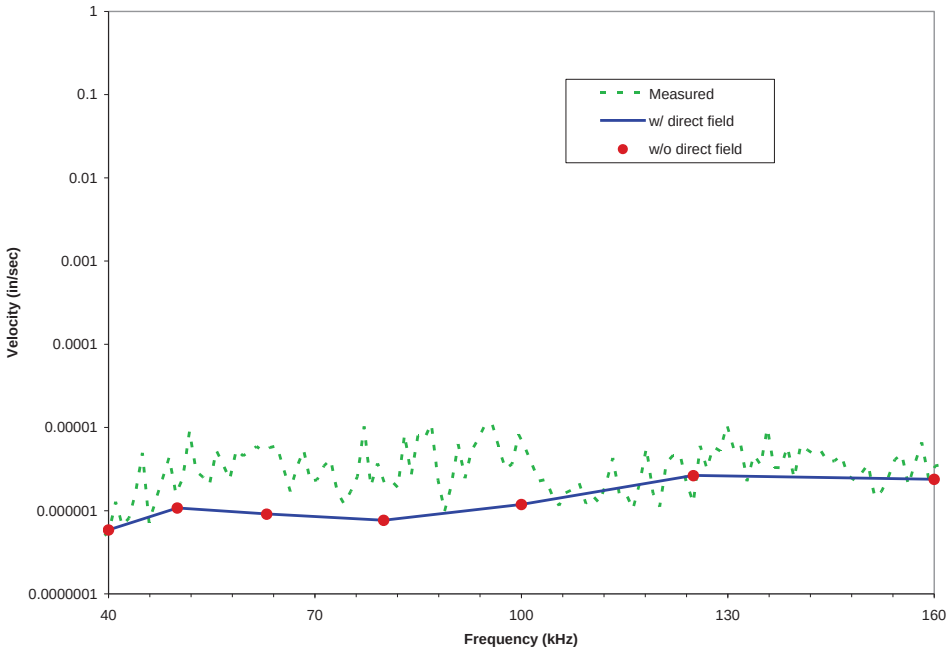

Figure A.6 Comparison at sensor 5

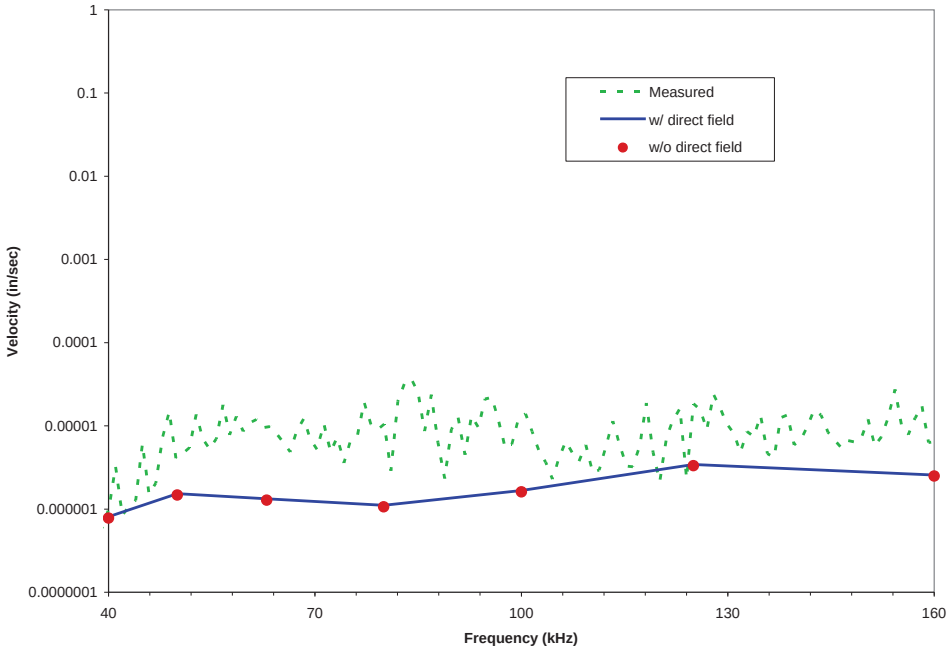

Figure A.7 Comparison at sensor 7

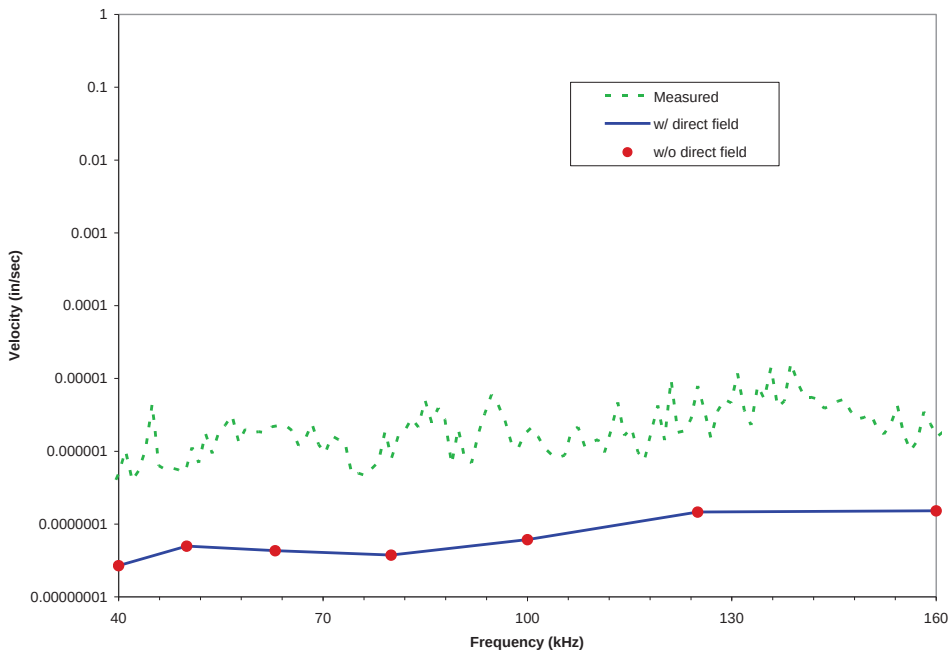

Figure A.8 Comparison at sensor 3

A.2 Effect of Input Power Computation

Finally, in order to illustrate the effect of the direct field, a synthesized example involving source and sensor locations that are next to each other is studied (note that this is similar to the actual case that was studied in the previous report). Again, source 10 case is considered. The correlated input power is obtained by trial and error since no measured response close to source 10 is available. A comparison of this estimated power to the measured power is shown in Figure A.9. Using this estimated input power, responses at all sensors are computed and these are compared to measured velocities in Figures A.10 - 16. As expected, better correlations are obtained at all sensors compared to the previously presented results in this report. Although the input power is generated by trial and error, it indicates that if more accurate input power is used (by placing the sensor close to source location), improved correlation between EnFlow predictions and measurements.

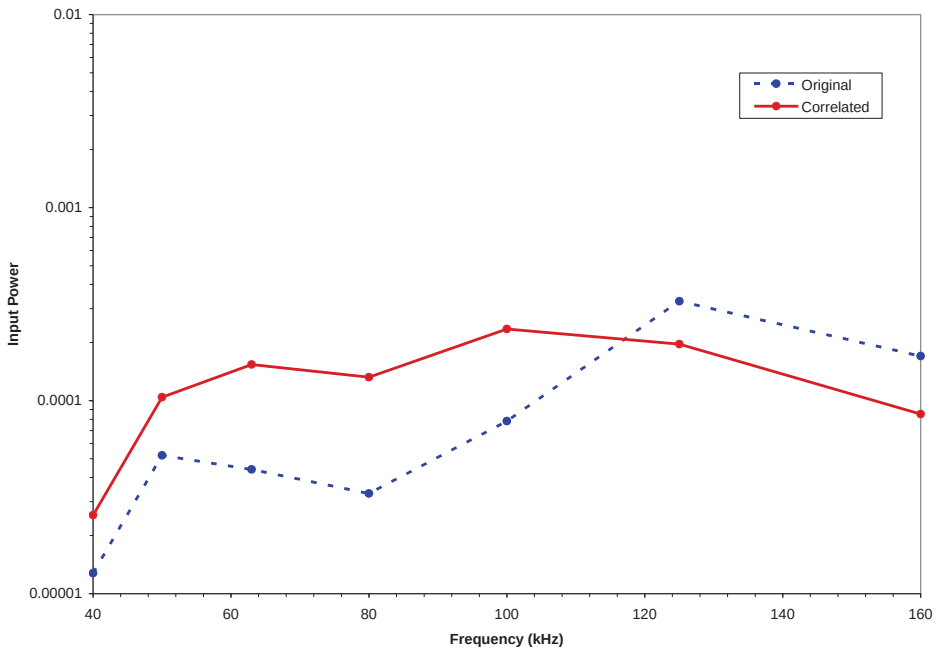

Figure A.9 Input power comparison at source 10

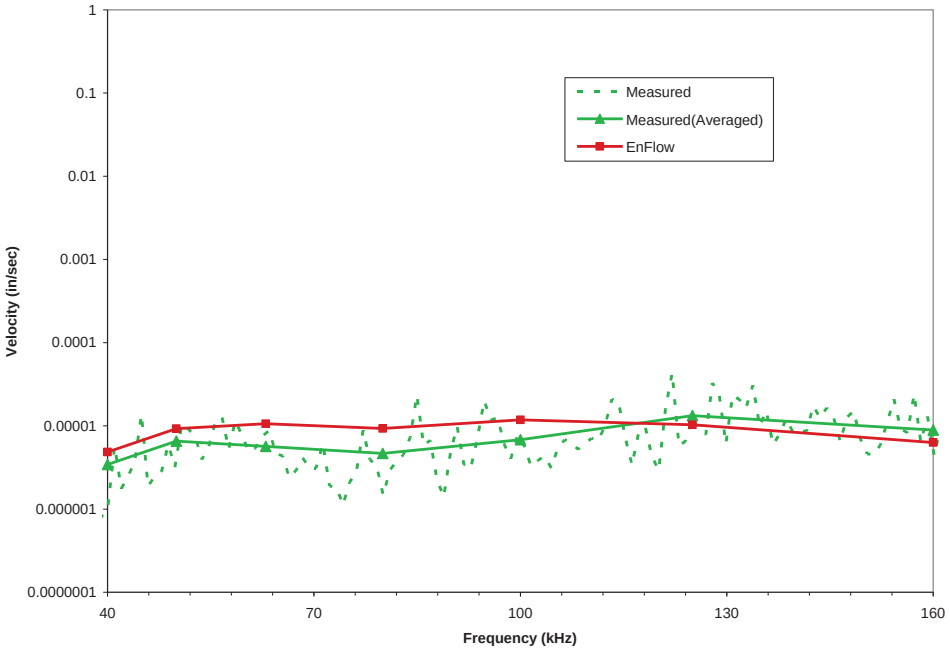

Figure A.10 Comparison at sensor 6

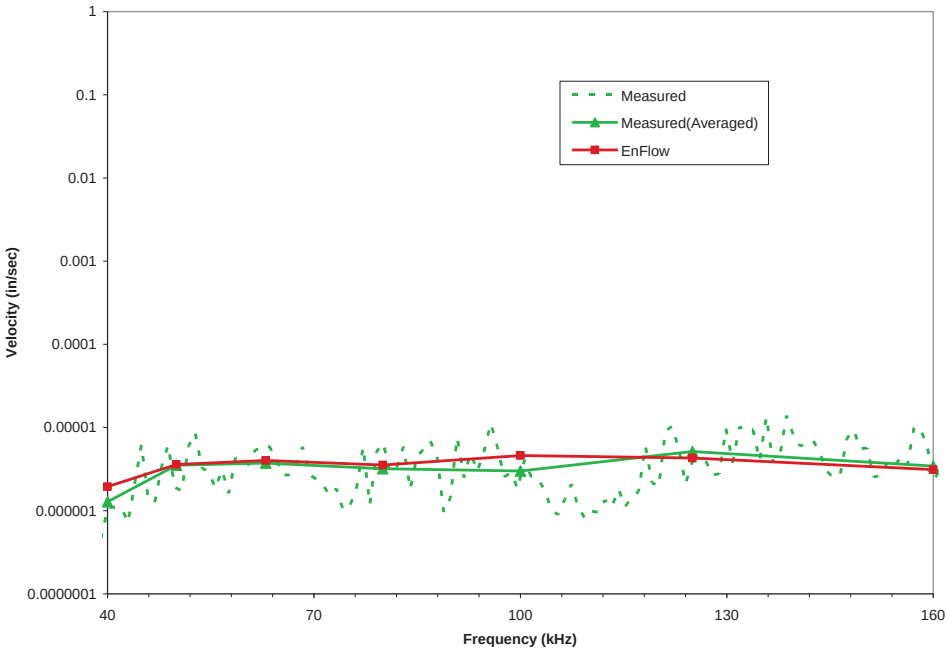

Figure A.11 Comparison at sensor 1

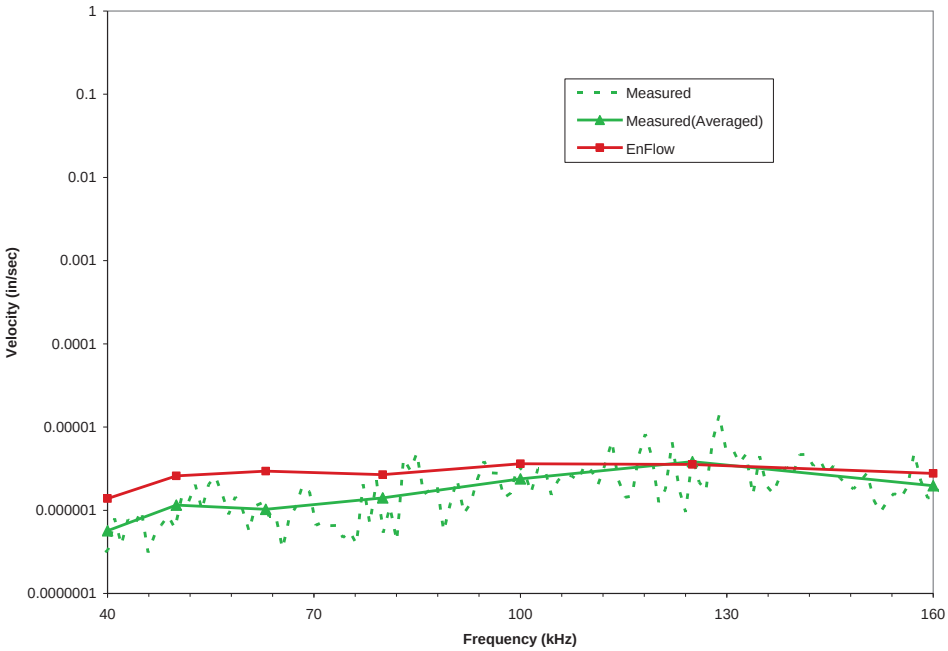

Figure A.12 Comparison at sensor 2

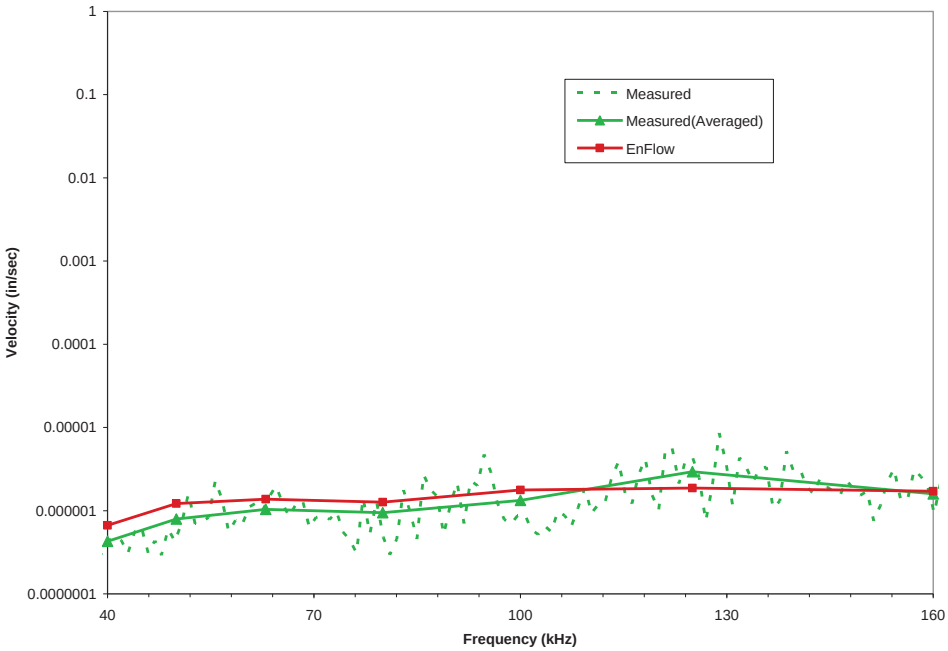

Figure A.13 Comparison at sensor 4

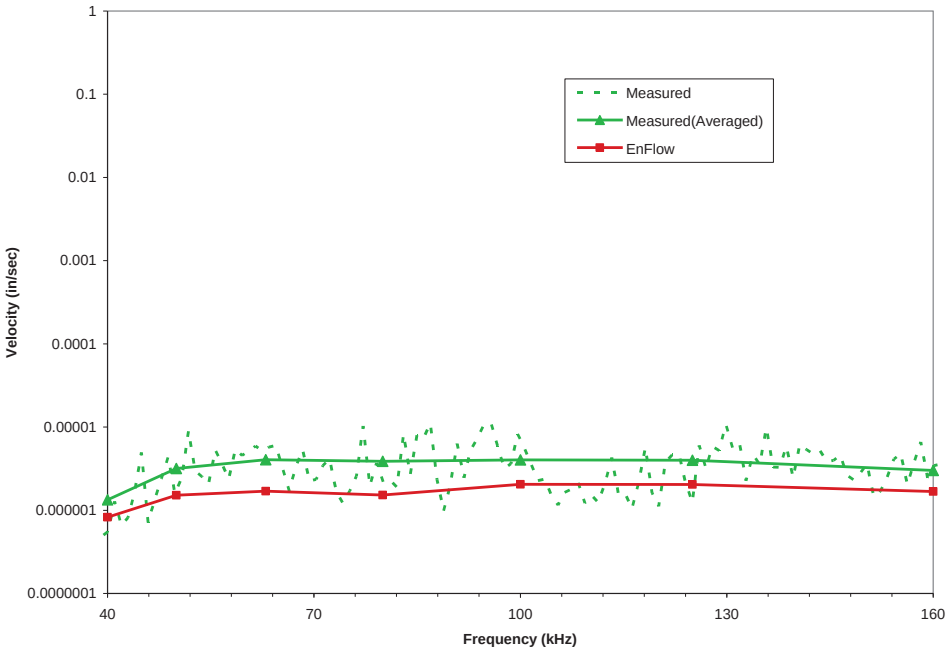

Figure A.14 Comparison at sensor 5

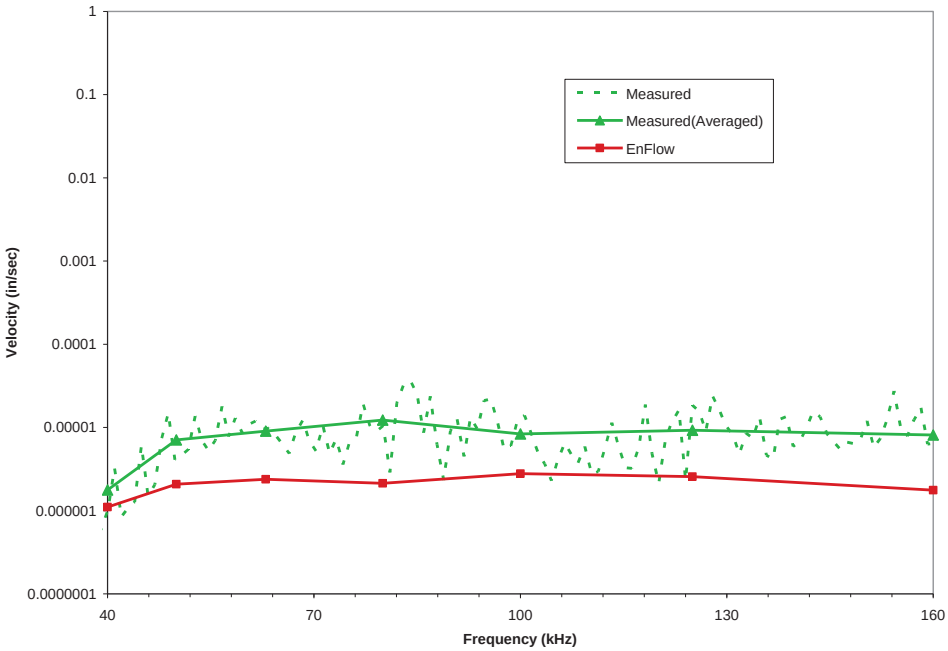

Figure A.15 Comparison at sensor 7

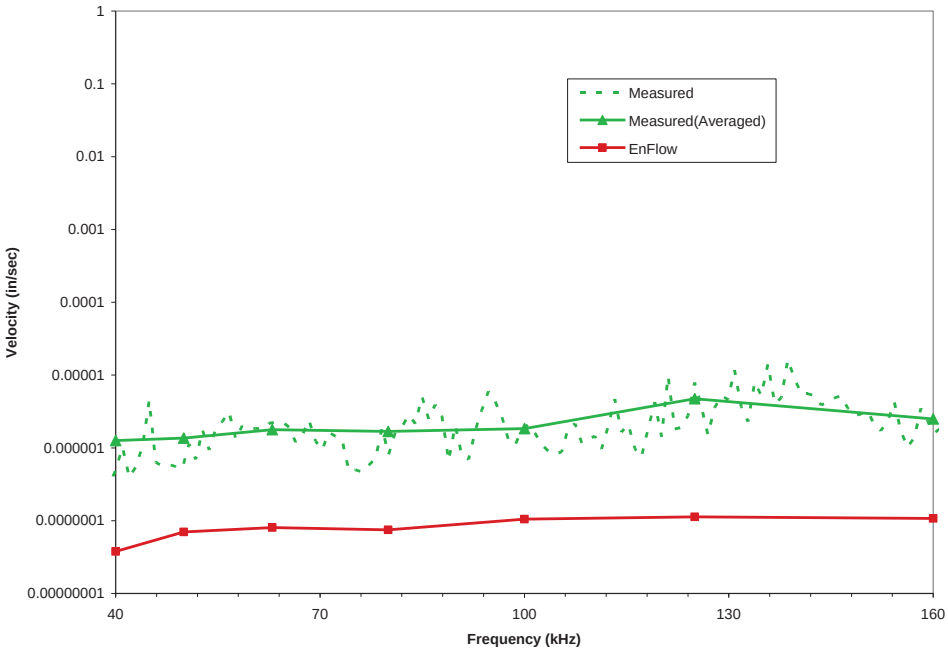

Figure A.16 Comparison at sensor 3

REPORT DOCUMENTATION PAGE

Form Approved
OMB No. 0704-0188

The public reporting burden for this collection of information is estimated to average 1 hour per response, including the time for reviewing instructions, searching existing data sources, gathering and maintaining the data needed, and completing and reviewing the collection of information. Send comments regarding this burden estimate or any other aspect of this collection of information, including suggestions for reducing this burden, to Department of Defense, Washington Headquarters Services, Directorate for Information Operations and Reports (0704-0188), 1215 Jefferson Davis Highway, Suite 1204, Arlington, VA 22202-4302. Respondents should be aware that notwithstanding any other provision of law, no person shall be subject to any penalty for failing to comply with a collection of information if it does not display a currently valid OMB control number.
PLEASE DO NOT RETURN YOUR FORM TO THE ABOVE ADDRESS.

1. REPORT DATE *(DD-MM-YYYY)*
01- 04 - 2014

2. REPORT TYPE
Contractor Report

3. DATES COVERED *(From - To)*

4. TITLE AND SUBTITLE
Calibration of International Space Station (ISS) Node 1 Vibro-Acoustic Model - Report 2

5a. CONTRACT NUMBER
NNL07AA00C

5b. GRANT NUMBER

5c. PROGRAM ELEMENT NUMBER

6. AUTHOR(S)
Zhang, Weiguo; Raveendra, Ravi

5d. PROJECT NUMBER

5e. TASK NUMBER
3-034CY2-3

5f. WORK UNIT NUMBER
401769.06.03.04.02.12

7. PERFORMING ORGANIZATION NAME(S) AND ADDRESS(ES)
NASA Langley Research Center
Hampton, Virginia 23681

8. PERFORMING ORGANIZATION REPORT NUMBER

9. SPONSORING/MONITORING AGENCY NAME(S) AND ADDRESS(ES)
National Aeronautics and Space Administration
Washington, DC 20546-0001

10. SPONSOR/MONITOR'S ACRONYM(S)
NASA

11. SPONSOR/MONITOR'S REPORT NUMBER(S)
NASA/CR-2014-218249

12. DISTRIBUTION/AVAILABILITY STATEMENT
Unclassified - Unlimited
Subject Category 16
Availability: NASA CASI (443) 757-5802

13. SUPPLEMENTARY NOTES
This work was performed by Comet Technology Corporation for Science Systems and Applications, Inc., under NASA contract NNL07AA00C.
Langley Technical Monitor: Eric I. Madaras

14. ABSTRACT
Reported here is the capability of the Energy Finite Element Method (E-FEM) to predict the vibro-acoustic sound fields within the International Space Station (ISS) Node 1 and to compare the results with simulated leak sounds. A series of electronically generated structural ultrasonic noise sources were created in the pressure wall to emulate leak signals at different locations of the Node 1 STA module during its period of storage at Stennis Space Center (SSC). The exact sound source profiles created within the pressure wall at the source were unknown, but were estimated from the closest sensor measurement. The E-FEM method represents a reverberant sound field calculation, and of importance to this application is the requirement to correctly handle the direct field effect of the sound generation. It was also important to be able to compute the sound energy fields in the ultrasonic frequency range. This report demonstrates the capability of this technology as applied to this type of application.

15. SUBJECT TERMS
Acoustics; Finite element method; International Space Station

16. SECURITY CLASSIFICATION OF:			17. LIMITATION OF ABSTRACT	18. NUMBER OF PAGES	19a. NAME OF RESPONSIBLE PERSON
a. REPORT	b. ABSTRACT	c. THIS PAGE			STI Help Desk (email: help@sti.nasa.gov)
U	U	U	UU	37	19b. TELEPHONE NUMBER *(Include area code)* (443) 757-5802

Standard Form 298 (Rev. 8-98)
Prescribed by ANSI Std. Z39.18